GEOLOGICA CARPATHICA, 2025, 76, 6, 459–483 https://doi.org/10.31577/GeolCarp.2025.25

Geology and thermal maturity of autochthonous Upper Cretaceous deposits on the southeastern margin of the Bohemian Massif

SLAVOMÍR NEHYBA[1,✉], EVA GERŠLOVÁ[2], VLADIMÍR OPLETAL[2,3], PETR SKUPIEN[2] and LUCIE UHROVÁ[4]

[1]Department of Geological Sciences, Faculty of Science, Masaryk University, Kotlářská 2, 611 37 Brno, Czech Republic
[2]Department of Geological Engineering, Technical University of Ostrava, 17. Listopadu 15/2172, 708 33 Ostrava, Czech Republic
[3]MND a.s., Úprkova 807/6, 695 01 Hodonín, Czech Republic
[4]Czech Geological Survey, Leitnerova 22, 602 00 Brno, Czech Republic

(Manuscript received August 7, 2025; accepted in revised form January 7, 2026; Associate Editor: Katarína Bónová)

Abstract: Knowledge of deposits of the Klement Formation (Upper Cretaceous) has been deriven solely from subsurface data in the southern Moravian territory of the Czech Republic. These deposits were deposited on a passive margin of the Neo-Tethys Ocean and a seaway continuation into the Bohemian Cretaceous Basin towards the north and northwest. Three recognised facies associations provide evidence of lower to middle shoreface to offshore depositional environments with role of storm events. Palynological studies of the deposits indicate a Late Albian age, which connect them with the initial Cretaceous transgression (Albian–Lower Cenomanian) onto the Bohemian Massif. The provenance from the eastern margin of the Bohemian Massif is proved and some potential source areas are evaluated. The principal and proximal source can be located in the Moravo–Silesian Zone (Brunovistulicum), which compose the crystalline basement of the Mesozoic deposits. More distant sources can be traced to the Moravian and Moldanubian units or to even more distant sources such as the Teplá–Barrandian or Lugicum units. A remarkable difference in provenance has been recognised when compared with the clastic Jurassic deposits of the Gresten and Nikolčice Formations known from the area under study. The base of the Klement Formation represents a composite, polyhistory surface and subaerial unconformity. The thicknesses of Cretaceous Klement Formation deposits is generally increasing eastwardly pointing to the general increase in basin depth in this direction. According to the Rock-Eval pyrolysis, organic matter was classified as kerogen type III. Based on parameter Tmax thermal maturity of the Klement Formation corresponds to immature stage which means that the sediments were not exposed to temperatures greater than 50 °C. The absence of a depth trend in thermal maturity suggests that the original position of the evaluated samples was changed tectonically and that burial to maximum depth occurred before the overthrust or the Western Carpathians.

Keywords: Klement Formation, Upper Cretaceous, borehole cores, provenance, depositional environment, thermal maturity

Introduction

The Bohemian Cretaceous Basin (BCB) belongs to the largest preserved sedimentary basin in the area of the Czech Republic and forms an important part of the Cretaceous System in Europe

The BCB was formed at the Central European interface of the Tethyan and Boreal provinces by the regional reactivation of primarily, older Variscan fault zones that dissect the Bohemian Massif and its surroundings. Following the global Cenomanian transgression a major part of Central Europe was flooded (Voigt et al. 2008), which led to formation of an island-dotted seaway formations, i.e., the so-called European Archipelago between the Tethyan and the Boreal realms (Csiki-Sava et al. 2015; Leszczyński & Nemec 2020). Marine passageways and straits commonly provided somewhat unusual conditions for sediment transport and accumulation (Longhitano 2013).

The BCB formed as a continental through shallow-marine siliciclastic system along reactivated, NW-trending faults of the Elbe fault zone. The stratigraphic range of the sedimentary infil of the basin is from Albian–Early Cenomanian to Santonian (Čech & Valečka 1991). The basin is filled by fluvial, lagoonal, deltaic, lacustrine and marine deposits (nearshore siliciclastics to offshore or hemipelagic marlstones and limestones).

The BCB is of great regional economic importance due to the natural resources it hosts. BCB deposits have been quarried for centuries; significant uranium accumulations were exploited starting from the middle of the last century, and the basin represents a hydrogeologically important aquifer system in the Czech Republic. These deposits represent a popular target for geological studies upon which geological literature on the basin is extended (Krejčí 1870; Malkovský et al. 1974;

✉ corresponding author: Slavomír Nehyba
slavek@sci.muni.cz

Klein et al. 1979; Čech et al. 1980; Skoček & Valečka 1983; Valečka & Skoček 1990; Uličný et al. 1997, 2009a, b; Čech 2011, and references therein).

However, slightly different situation existed on the SE periphery of the BCB, where the Bohemian Massif passed into a passive margin of the Neotethys Ocean. Stráník et al. (1996) describe outer-shelf units of Turonian to Coniacian age from several deep boreholes, but post-Mesozoic erosion along the SE marging of the Bohemian Massif and thrusting at the frontal zone of the West Carpathians preclude the detailed reconstruction of depositional patterns between the BCB and the region further south-east (Csontos & Vörös 2004; Schmid et al. 2008; Mitchel et al. 2010). With exceptions of small exposures near Brno, the Upper Cretaceous deposits in the southern Moravian and northeastern Austrian regions (i.e. southeastern slopes of the Bohemian Massif) are deeply buried below the Neogene Alpine–Carpathian Foredeep and the Carpathian thrustbelt units. Such deposits are in the local geological literature designated as the autochthonous Upper Cretaceous deposits, see Fig. 1A (Pícha et al. 2006; Stráník et al. 2021).

The southern Moravia and northern Austria are prospective areas in terms of hydrocarbon production. A comprehensive overview of hydrocarbon systems in the Carpathian Belt and its foreland along the southeastern margin of the Bohemian Massif was provided by Ciprys et al. (1995), Pícha et al. (2006), and Mayer & Sachsenhofer (2013). The potential source rocks investigated are primarily the Middle Devonian and Upper Carboniferous, and Upper Jurassic and Lower Oligocene successions (Krejčí et al. 1994, 1996; Geršlová et al. 2015; Jirman et al. 2019; Opletal et al. 2019; Körmös et al. 2021; Rybár & Kotulová 2023), or the Miocene deposits (Geršlová et al. 2022). Although it is not probable, that Cretaceous deposits could be potential source rocks, due to low TOC, but they carry information about thermal maturity and thus provide a crucial element in the basin modelling especially for calibrating the subsidence curve for the Mikulov Marls. However, no systematic study of thermal maturation has been conducted yet on these deposits.

Our aim is to provide more detailed information about the Upper Cretaceous deposits of the Klement Formation (KF)

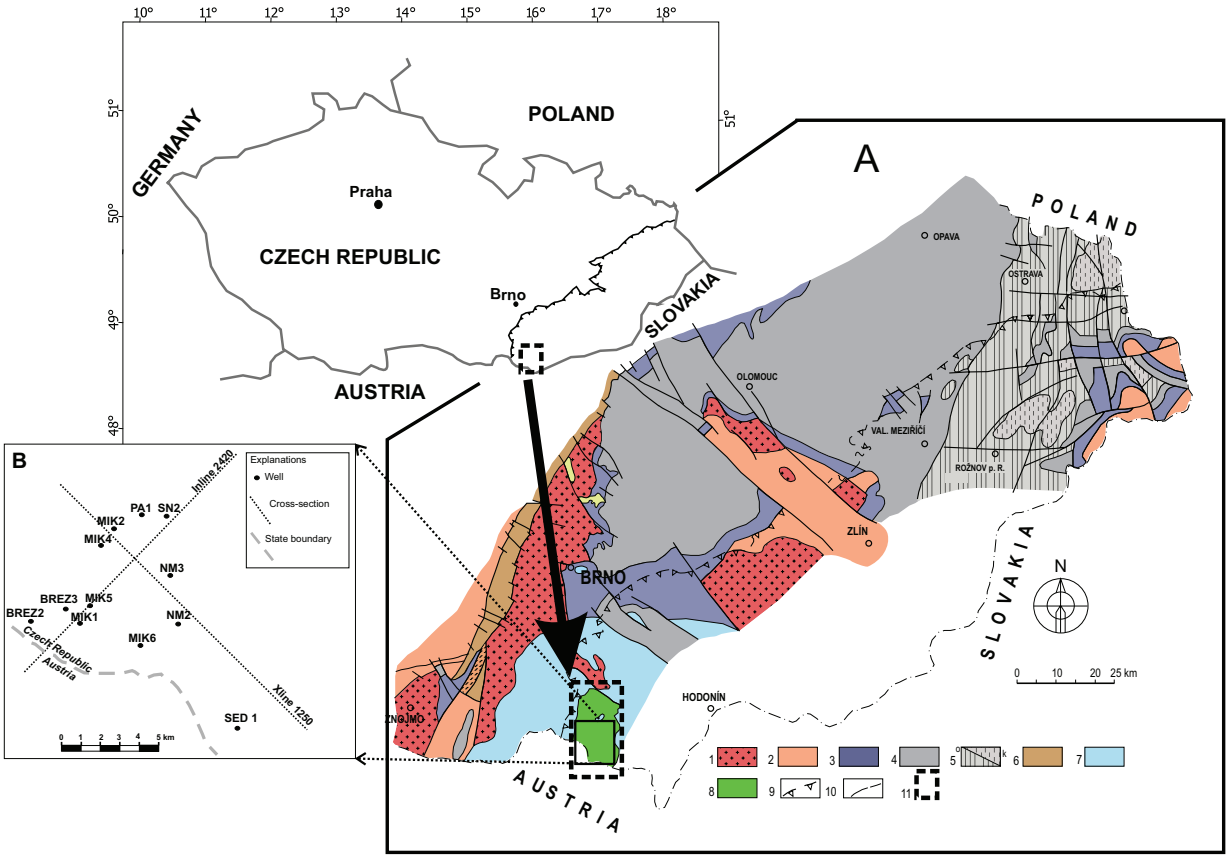

Fig. 1. A — Geological map of the Pre-Neogene basement of the eastern slopes of the Bohemian Massif (Stráník et al. 2021 modified). Explanation: 1 – magmatic rocks of Brunovistulicum (Precambrian), 2 – metamorphic rocks of the Brunovistulicum, Moldanubian and Moravian units, 3 – Cambrian to Upper Devonian deposits, 4 – Lower Carboniferous deposits (Culmian), 5 – Upper Carboniferous coal-bearing deposits (a – Ostrava Fm., b – Karviná Fm.), 6 – Permo–Carboniferous deposits, 7 – autochthonous Jurassic deposits, 8 – autochthonous Cretaceous deposits (Klement Fm.), 9 – front of the nappes of the Western Carpathian Flysch Zone, 10 – faults, 11 – investigated area. **B** — Geographic location of the area under study with position of the petroleum industry wells which confirmed deposits of the Klement Formation and cross-sections. Abbreviations are used for the designation of the wells i.e. MIK 1, 2, 4, 5, 6 as Mikulov 1, 2, 4, 5, 6; BREZ 2, 3 as Březí 2, 3; NM 2, 3 as Nové Mlýny 2, 3; SED 1 as Sedlec 1; SN2 as Strachotín 2; PA1 as Pavlov 1.

in the Southern Moravian region based on the study of borehole cores and geological analyses 3D seismic data acquired for oil and gas exploration purposes. As an output the characterization of the depositional environment, source area, thermal maturity, and properties of source rocks. A simplified map of the studied area is presented in Fig. 1A, B, where the geological map of the Pre-Neogene basement of the eastern slopes of the Bohemian Massif is also indicated (Stráník et al. 2021 modified).

Geological setting

The studied area is situated along the border between the West Carpathian belt and the West European plate; represented by the eastern margin of the Hercynian Bohemian Massif (Schmid et al. 2008; Hrubcová et al. 2010). The basement is formed by the crystalline rocks of the Proterozoic Brunovistulicum and its Paleozoic–Neogene sedimentary cover (Stráník et al. 2021). A generalised stratigraphic scheme is shown in Fig. 2. In the Carpathian foreland of Moravia and northeastern Austria, the Mesozoic to Cenozoic Tethyan–Alpine cycle began in the Early to Middle Jurassic continental rifting and extension. These processes led to the opening of the Dyje–Thaya depression, a northwest–southeastwardly oriented structure parallel with to the wrench fault system on the southwestern side of the Bohemian Massif (Pícha et al. 2006). A marine transgression and the formation of carbonate-dominated passive continental margins followed in the latest Middle and Late Jurassic (Pícha et al. 2006).

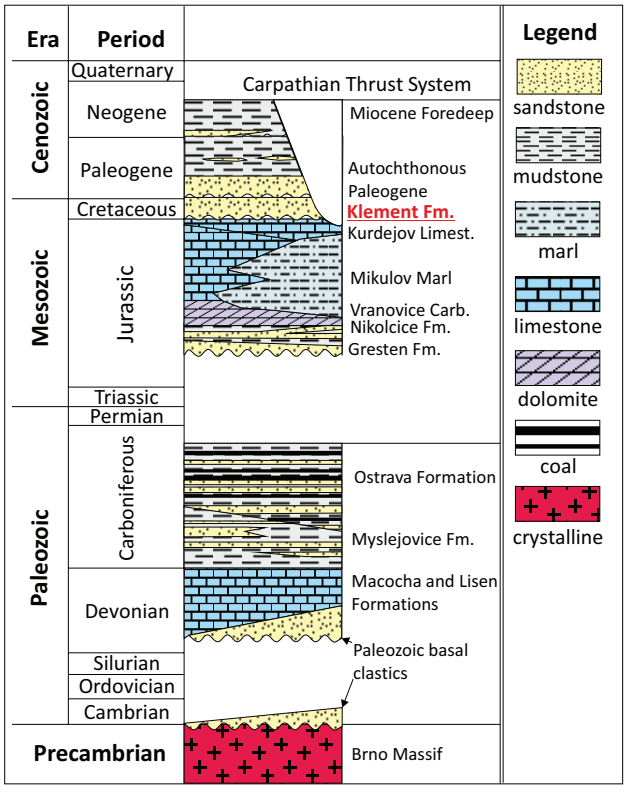

Fig. 2. Generalized stratigraphic scheme of the autochthonous units in the area under study (SE slopes of the Bohemian Massif in SE Moravia) (modified after Pícha et al. 2006 and Stráník et al. 2021).

The Jurassic sequence begins with synrift terrestrial fluvial and deltaic deposits of the Gresten Formation (Bajocian–Bathonian) (Wessely 1988; Nehyba & Opletal 2016). A new marine transgression during the Callovian led to the development of the predominantly noncarbonatic depositional environment with deposition of the dolomitic sandstones of the Nikolčice Formation (Callovian) (Adámek 2005; Nehyba & Opletal 2017). During the Oxfordian clastic sedimentation gradually gave way to a predominantly carbonate depositional environment (e.g., the Vranovice Limestones and Dolomites), followed by tectonic downwarping of the Jurassic passive continental margin/shelf in the southeastern part of the area. Whereas deeper marine anoxic basin with monotonous sedimentation of dark, organic-rich Mikulov Marls developed in the southeast, shallow marine carbonate deposition (high-energy carbonate platform) formed in the northwest (the Altenmarkt Group). The Mikulov Marls pass upwards into a formation of organodetrital limestones and dolomites called the Kurdějov Limestones (Tithonian). Further organodetrital sedimentation continued with partly dolomitised limestones, which are equivalent to the allochthonous Ernstbrunn Limestones known from the Outer Klippen in northeastern Austria and southern Moravia (Pícha et al. 2006).

During most of the Early Cretaceous, the area of southern Moravia and northeastern Austria was uplifted and Jurassic deposits were eroded and karstified. Marine carbonate sedimentation marginally resumed during the Aptian–Albian, as evidenced by rare occurences of limestone beds described by Krystek & Samuel (1978), Řehánek (1984), and Adámek (1986).

A major global transgression in Cenomanian flooded most of the European platform, including its marginal sections adjacent to the Tethyan realm and culminated in the Upper Turonian (Adámek & Stránik 2021). The Upper Cretaceous deposits are known from the Dyje–Thaya depression from numerous boreholes (Pícha et al. 2006). Řehánek (1978) described these deposits as the sandy-glauconitic series. Based on study of several deep boreholes, Adámek (1986) interpreted these deposits as the KF (Turonian to Maastrichtian) with considerable lithological variability. The lower part is dominated by gray sandstone with glauconite and the upper part is characterised by calcareous claystone and siltstone with interbeds of sandy limestone and sandstone. Assemblages of foraminifers and calcareous nannofossils are very poor and rarely preserved, indicating an age of Cenomanian to Maastrichtian (Stráník et al. 1996), and/or Late Cenomanian to Early Campanian (Řehánek 1995). The depositional environment was located in a deeper sublitoral zone where bottom currents, bioturbation, and oxidic conditions played important role.

The total thickness of the KF highly varies, which is explained by the role of the vertically diversified basin bottom

and postdepositional erosion. The maximum thickness in the studied area was 216 metres (borehole Nové Mlýny 2); however, a maximum thickness of 517 metres was recorded in the well Ameis-1 in Austria (Stráník et al. 1996). These Upper Cretaceous deposits represent a transitional facies between the epicontinental deposits of the boreal sea of northern Europe, such as the Brezno Formation of the Bohemian Massif and the coeval deposits of the Tethyan continental margins (Pícha et al. 2006).

The Late Cretaceous to Early Miocene deposits of southern Moravia are a part of the foreland depositional system, which gradually evolved along the front of the Alpine–Carpathian thrust belt after the Late Cretaceous collision of Apulia with Eurasia, deformation of the inner zones of Alps and Carpathians (Austrian phase), and conversion of passive Tethyan margins into active continental margins (Pícha et al. 2006).

Finally, the area underwent extensive peneplanation and subsequent deposition during the thrusting of the Western Carpathians and related formation of the Western Carpathian Foredeep (e.g., the Miocene peripheral foreland basin; Nehyba & Šikula 2007).

Methods of study

The whole Cretaceous depositional system in the studied area is deeply buried under the Carpathian Thrust Units and sediments of the Carpathian Foredeep Basin; no outcrops are available. Therefore, a geophysical dataset was analyzed in Schlumberger Petrel software to interpret the 3D seismic data and determine the areal extent, thicknesses, and depositional and tectonic evolutions of the studied unit. The 3D seismic data were acquired between 2013–2014 by Geofyzika Krakow and in 2016 seisimic processing by MND a.s. processing center for interpretation. Vibroseis technology was used for seismic acquisition with a final nominal fold of 150–200 in 25 meter size of the processing bin. Total number of the source points was 8770 with source point interval 50 m and receiver interval 50 m with maximum offset 5275 m. The trace length was 6000 ms with 2 ms sample interval. The time depth conversion was done using the vertical seismic profiling data from deep boreholes (wells) with calibration using sonic and density data from the well logging. The pre-stack time migration time processing version was used for seismic interpretation. The seismic interpretation was done using the best practices of 3D seismic interpretation (Brown 2004), where time data were calibrated to depths using the vertical seismic profiling, check-shots and synthetic seismograms (where sonic and density logs were available) data. The deep boreholes results (cores, well logs, well cuttings etc.) were used for stratigraphy definitions in depth domain. The 3D data cover the major part of autochthonous Cretaceous depositional sequence, excluding the deepest part, which dip steeply under the Carpathian thrust units and the Vienna basin in depths greater than 4000 meters. This southeast area of the studied region was partially analysed trough the 2D seismic dataset where possible; but at its deepest section the thickness of the Carpathian thrust units is more than 3500 meters, leaving the Cretaceous depositional system largely uninterpreted. Such thickness compounded by the complex geometry of the thrust units cause significant attenuation of seismic waves; this leads to a quick decrease of seismic signal to noise ratio, which makes the proper geological interpretation of such data exceedingly difficult, if not nearly impossible (Hrubcová et al. 2010).

The study was carried out on 9 cores from 6 wells: i.e. Mikulov 5 (core 1), Nové Mlyny 2 (cores 2, 3), Nové Mlýny 3 (cores 4c, 5, 6), Pavlov 1 (core 1), Sedlec 1 (core 18) and Strachotín 2 (core 7). The position of the boreholes is illustrated in Fig. 1B. The quality and quantity (thickness) of cores varied significantly.

The largest "continuous" thickness of the cores was 9.5 meters, but the average thickness reaches mostly only a few meters. Altogether, more than 34 meters of cores were logged. Facies analysis follows Walker & James (1992) principles. Further information was provided by the evaluation of available wire-line logs owned and acquired by MND a.s. in individual wells, e.g., spontaneous potential (SP), resistivity (Rag 2, 12) and gamma-ray (gamma-API) (Rider 1991).

Grain size analysis was provided on one unlithified sample using combined sieving and laser methods. A Retsch AS200 sieving machine analysed the coarser fraction (4–0.063mm, wet sieving), and a Cilas 1064 laser diffraction granulometer was used to analyse the finer fraction (0.0001–0.5mm). Ultrasonic dispersion, distillate water, and washing in sodium polyphosphate were applied before analyses to avoid flocculation among the particles analysed (Dinis & Castalho 2012).

Assemblages of heavy minerals were evaluated in the grain-size fraction 0.063–0.125 mm (2 samples, core 1, well Mikulov 5). Garnet, zircon, and rutile are relatively stable during diagenesis and have a wide compositional range; they should thus be further evaluated in greater detail. Zircon studies (outer morphology, colour, presence of older cores, inclusions and zoning, typology, and elongation) were provided on 162 grains. Electron microprobe analyses of the garnet (61 grains) and rutile (25 grains) were evaluated with a CAMECA SX electron microprobe analyser (Faculty of Science, Masaryk University, Brno, Czech Republic).

U–Th–Pb zircon analyses were performed by LA–ICP–MS using an Analyte Excite 193 nm excimer laser (Photon Machines) with a two-volume HelEx cell coupled to an Agilent 7900x ICP–MS at the Czech Geological Survey (sample core 1, Mikulov 5 well). Ablation was conducted in He (0.8 l min^{-1}) at 5 Hz with a 25 μm spot and 7.6 J cm^{-2} fluence. Zircon 91500 (TIMS $^{207}Pb/^{206}Pb$ age = 1065.4 ± 0.3 Ma; Wiedenbeck et al. 1995) was used as the primary standard, and Plešovice (mean ID-TIMS U–Pb age = 337.13 ± 0.37 Ma; Sláma et al. 2008) and GJ-1 (TIMS $^{207}Pb/^{206}Pb$ age = 608.5 ± 0.4 Ma; Jackson et al. 2004) as secondary standards, analysed every ten spots to monitor drift. Data reduction in Iolite software (Paton et al. 2010) included background and laser-induced fractionation corrections. Plešovice and GJ-1 yielded concordant ages of 337 ± 2 Ma and 602 ± 3 Ma (2σ).

The gamma-ray spectra (GRS) were measured by a GR-320 enviSPEC laboratory spectrometer with a 3×3 in. NaI(Tl) scintillation detector (Exploranium, Canada). Counts per second in selected energy windows were directly converted to concentrations of K (%), U (ppm) and Th (ppm). One measurement of 30 minutes was performed for each measured sample (40 samples – min. 300 g), and the total radioactivity i.e. "standard gamma ray" labeled as SGR was estimated from the following: SGR [API]=16.32×K (%)+8.09×U (ppm) +3.93×Th (ppm) (API/American Petroleum Institute units) (Rider 1991). Twenty samples were analysed (2 samples – wells Strachotín 2 and Sedlec 1 each, 3 samples – wells Mikulov 5 and Pavlov 1 each, 4 samples – well Nové Mlýny 2, 6 samples – well Nové Mlýny 3).

Palynological sample was obtained from the core of the borehole Mikulov 5 (depth 1610,4 m – top part of the core). After washing and drying, 15–20 g of rock was treated with HCl and HF. Sieving was performed using a 15 µm nylon mesh, and the samples were centrifuged to concentrate the residues. Oxidation was not used. Three slides from each sample were prepared. The palynofacies analysis and photo-documentation were carried out using Olympus BX60 optical microscope and NIS-Elements 3.1. software. The formalised non-calcareous dinoflagellate taxa are fully referenced in both Fensome & Williams (2004) and Williams et al. (2017). The permanent palynological mounts are stored at the Department of Geological Engineering at the VSB – Technical University of Ostrava. The amount of kerogen in the palynological slides was analysed to obtain paleoenvironmental information. More than 500 particles were counted in each sample following Tyson (1995), such as: phytoclasts (brown and black material, cuticles), amorphous organic material (AOM), spores and pollen grains, dinoflagellate cysts and other algae, acritarchs, and foraminiferal test linings.

Analyses of the source rock were conducted on the 5 samples taken from 5 exploration wells. All the samples collected were analysed for total organic carbon (TOC) and Rock-Eval pyrolysis. Archival results from Rock-Eval pyrolysis (10 in total) from the underlying Jurassic units were used to determine the thermal maturity profile (Table 1). The Rock-Eval 6 instrument was used to determine the free hydrocarbons content S1 [mg HC/g rock], remaining hydrocarbon potential S2 [mg HC/g rock] and temperature of the maximum of the S2 peak Tmax [°C]. The production index (PI=S1/(S1+S2)) and the hydrogen index (HI=100×S2/TOC [mg HC/g TOC]) were calculated following Lafargue et al. (1998).

Results

Seismic interpretation

Several key horizons (Figs. 3 and 4) were interpreted using seismic data for a better understanding of the regional

Table 1: Descriptive summary list of lithofacies of the studied deposits distinguished in the studied cores of the Klement Formation.

Symbol	Description	Interpretation
Sl	Light grey, medium coarse grained sandstone, faint low inclined planar parallel stratification, relatively well sorted, Bioturbation index 1–3. Medium to thick bedded.	Horizontal planar parallel-lamination suggests deposition by transitional to upper flow regime unidirectional currents, storm deposits.
Sb	Light grey to whitish, green, very fine, fine to medium grained sandstone, relatively well sorted, glauconitic. Structureless to mottled. Bioturbation index 4–5. Rarely recognised fish tooth. Medium to thick bedded, mostly gradual base and top, rarely sharp inclined base.	Action of organisms obliterating primary structures.
Sm	Light grey, green, medium to coarse sandstone, structureless, Bioturbation index 1–3. Medium to thick bedded, gradual base and top.	Rapid deposition from unidirectional heavily laden current.
HS	Sandstone dominated heterolith. Greenish grey, light grey very fine, medium to coarse grained sandstone, irregular flasers or laminae of grey mudstone. BI index highly varies 2–4. Sometimes faint or mottled remnants of low inclined laminations. Two varieties glauconitic or non-glauconitic.	Deposition above storm wave base, subsequent burrowing obliterated the primary sedimentary structures, oxygenated condition.
HM	Mudstone dominated heterolith, dark grey claystone with admixture of light grey siltstone and very fine sandstone. Bioturbation index varies 3–5. Sometimes deformed. Two varieties – micaceous or glauconitic. Fossiliferous, admixture of fossilified plant remnants. Thick to thin bedded. Mostly transitional both top and base of the bed.	Deposition below storm wave base, mixed shelfal current and suspension setting subsequent burrowing obliterated the primary sedimentary structures, oxygenated condition, more distal environment comparing to HS.
FSb	Thoroughly bioturbated silty to very fine sandy mudstone, mottled.	Primary sedimentary structures destroyed by bioturbation. Deposition bellow storm wave base, well-oxygenated productive conditions, more distal deposits compared to Sb.
Fb	Mudstone, silty claystone, massive or mottled, trace fossils only along base of bed, very rarely preserved remnants of planar parallel lamination. Bioturbation index 4–6.	Primary sedimentary structures destroyed by bioturbation. Deposition bellow storm wave base, well-oxygenated productive conditions, more distal deposits compared to FSb.
Fm	Massive silty claystone/marlstone.	Deposition from suspension, offshore deposits, influence biogenic production in surface waters, low-oxygenated condition evidenced by limited or absent bioturbation.

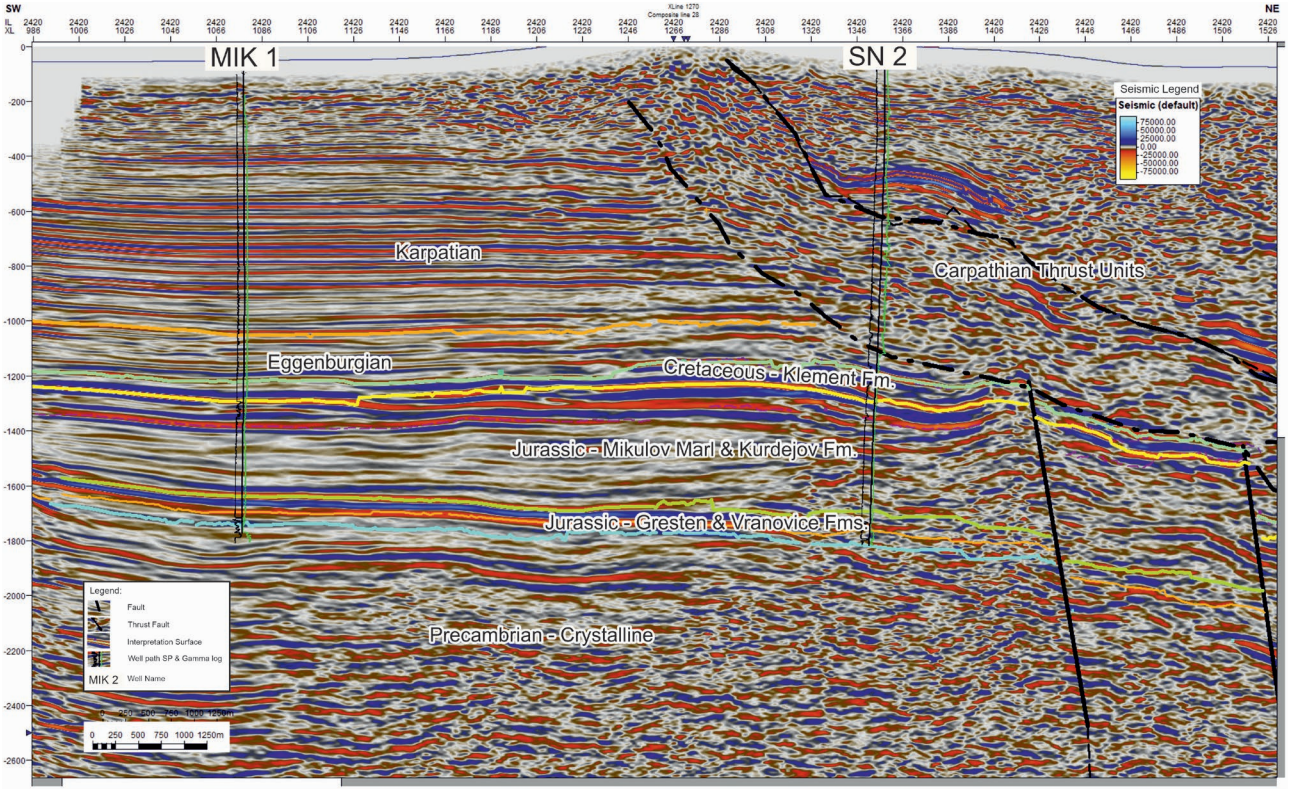

Fig. 3. The interpreted seismic along Inline 2420 on Fig. 1. The line is approximately NE–SW oriented.

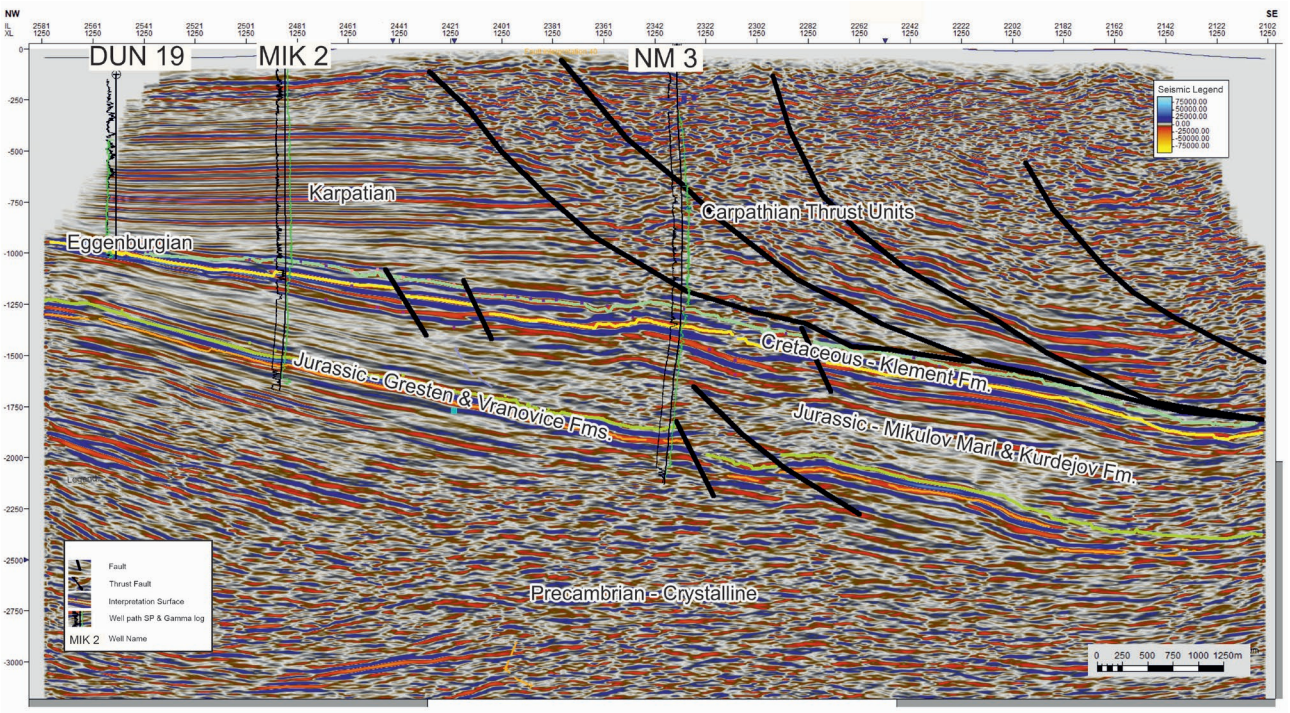

Fig. 4. The interpreted seismic along Xline 1250 on Fig. 1. The line is approximately NW–SE oriented.

geological setting and processes related to the deposition of Cretaceous sediments studied. Analyses were conducted starting with the top of the crystalline basement of Brunovistulicum (Precambrian) (orange interpretation) formed by mostly granodiorites. Directly overlying the crystalline basement is the Jurassic depositional sequence, beggining with the Gresten, Nikolčice and Vranovice Formations (the bright green interpretation representing their top), which were followed by the deposition of the Upper Jurassic Mikulov Marls. The final stage of the Jurassic depositional sequence is represented by the Kurdějov limestones (the yellow interpretation representing their top), which also serves as a basement for the studied Cretaceous depositional sequence. The complete Cretaceous sequence (light green interpretation representing the top of Cretaceous) is formed by high velocity greywackes (3600–3900 m/s measured during VSP in well Pavlov 1). Therefore, to interpret the top of Cretaceous deposits, the hard kick (an increase of acoustic impedance) aspect of the amplitude was used, as the deposits are usually overlain by slower Miocene sediments. Also, for the base of Cretaceous deposits, the hard kick part of the amplitude was used as it is directly overlying the Kurdějov limestones with velocities of approximately 6000 m/s and higher.

The interpretation and depth conversion of the Cretaceous depositional system is slightly complicated by the changing cap rocks in the area. Whereas in the northwest part of the studied area, the cap rocks are formed by the sub-horizontal layered autochthonous Miocene deposits, in the southeastern part, cap rocks compose the very complex system of Carpathian thrust units (Fig. 5).

The Carpathian thrust system is also significantly affecting the tectonic regime of the area. The older normal fault system of the Jurassic rifting stage (normal faults that generally strike southwest–northeastwardly) was reactivated during the thrusting and contributed to the recent tectonic style dominated by minor thrust faulting within the Pre-Cenozoic deposits directly under the Carpathian thrust units while keeping the normal fault Mesozoic tectonic pattern in the northwestern part before the front of the Carpathian thrust. Moreover, the original dip of the platform depositional system increases in the southeast direction due to flexural subsidence caused by the thickening of the thrusts of the Carpathian Nappes System (Figs. 3, 4).

Whereas the shape of the body of the Cretaceous sediments is concerned, it is obvious that in the northwest direction these sediments were gradually eroded along the line (between wells Brez2 and Sn1) during the Lower Miocene (Eggenburgian)

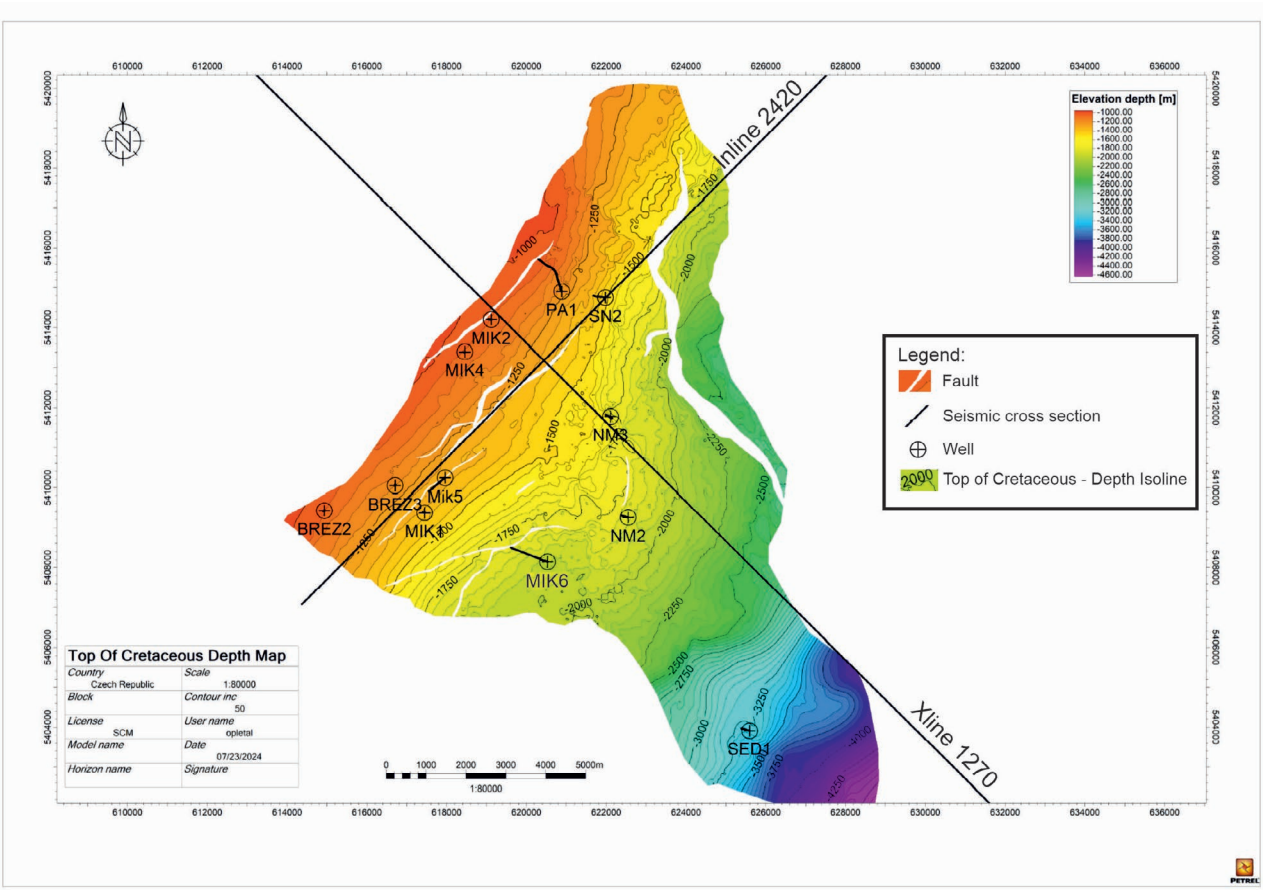

Fig. 5. Depth map on top of Cretaceous deposits of the Klement Fm. with highlighted faults and proposed limits of recognised areal extend of the Cretaceous deposits.

where they were observed incorporated in basal Eggenburgian sandstones. In the southeast, east directions the Cretaceous sediment thickness (Fig. 6) generally increases. But whereas in the eastward it is abruptly eroded/torn out by the deeply seated Carpathian thrust units, in the southeast direction it continues less steeply under the Carpathian thrust units down to the depths below the resolution of the available seismic dataset. Northward, the Cretaceous deposits have been completely eroded by subsequent Paleogene erosional/depositional events leading to the formation of Vranovice Paleovalley (not shown on presented sesmic sections).

Facies analysis

The lithofacies of the studied succession are summarised in Table 1 and organised into three facies associations (FA). Examples of lithofacies are presented in Fig. 7. Although it uses the high fold seismic acquisition, the 3D seismic interpretation unfortunately does not offer the frequency response to allow reliable interpretation of individual facies associations.

FA 1 consists of three lithofacies, i.e., Fb, FSb, and Fm, which represent mudstones with significant variations in admixture of very fine sand and intense bioturbation. Whereas biogenic reworking is common throughout the entire facies of Fb and FSb, it was absent in Fm. Facies Fb, FSb and Fm mostly gradationally underlie and overlie each other.

FA 2 consists of two lithofacies, i.e., HS and HM, which represent heteroliths with significant variations in the grain size of the dominant component. The level of intensity of bioturbation is generally middle to high (BI 2-5) (Taylor & Goldring 1993). Facies HS and HM are relatively rare. Facies HS typically covers facies Sb and is covered by facies FS or HM.

FA 3 consists of three lithofacies, i.e., Sb, Sm and Sl, ranging from completely bioturbated and/or structureless to sandstones with preserved primary sedimentary structures. The grain size varied from very fine up to medium to coarse grained and the bioturbation intensity varied significantly from low to high.

Interpretation: The fine-grained nature of FA 1 indicates a low-energy depositional environment beyond the influence of most current or wave processes. The rare sandstone content and laminae, however, might reflect exceptional storm events as possible distal tempestites (Johnson & Baldwin 1986). The deposits were interpreted as offshore deposits, i.e., proximal and distal shelf.

The fine-grained nature of the sediments, combined with a high degree of bioturbation and heterolithic fabric, reflects

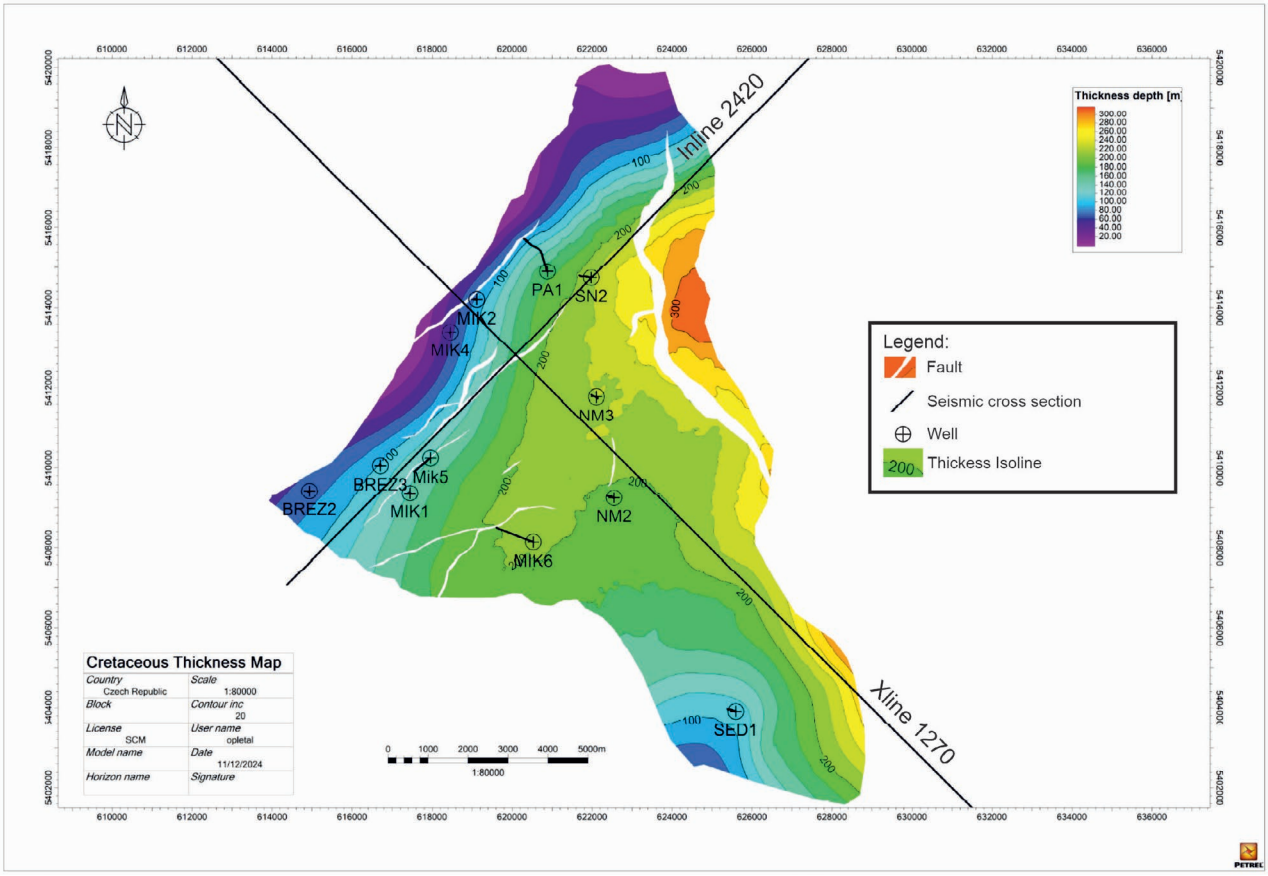

Fig. 6. Thickness map of the Cretaceous deposits of the Klement Fm. with highlighted faults and proposed limits of recognised areal extend of the Cretaceous deposits.

Fig. 7. Selected examples of lithofacies: **A** — lithofacies Sl; **B** — lithofacies Sm; **C** — lithofacies Sb; **D** — lithofacies Hs; **E** — lithofacies Hm; **F** — lithofacies Fm; **G** — lithofacies FSb; **H** — lithofacies Fb.

sedimentation in a transitional zone and upper offshore setting of FA 2 (Baniak et al. 2013). Features characteristic of rapid sedimentation (i.e., small ball and pillow structures) are rare. The sand sized sediment was derived from the shoreface (partly FA 3) through possible storm events. Similarly, a relic planar parallel lamination was interpreted as a distal tempestite. Evidence of a tide affection was missing (Rossi et al. 2017). Due to the infrequent nature of storm events, these sandy event beds were bioturbated during fair weather periods (MacEachern & Pemberton 1992).

The fine-grained nature of FA 3 combined with remnants of the primary sedimentary structures of lithofacies Sl indicates that sedimentation was affected by infaunal reworking. The local existence of stratification suggests high-wave energies and most probably represents storm deposits (Harms et al. 1975; Leckie & Walker 1982; Rossi et al. 2017). The high intensity of bioturbation in Sb combined with a general lack of primary sedimentary structures reveals that deposition was exceeded by the rate of infaunal reworking; it suggests either limited storm influence or considerable time between storm events (Baniak et al. 2013). Remnant low-angle parallel lamination was interpreted as a distal tempestite (storm-bed) (MacEachern & Pemberton 1992). A lack of sedimentary structures in lithofacies Sm points to rapid deposition and well sorting of the material. Moreover, biogenic activity obliterated the primary sedimentary structures. Continuously migrating bedforms limit animal colonisation (Baniak et al. 2013).

The general coarsening upward trend of FA 3, combined with the reduced intensity of bioturbation levels from intense to moderate or low (BI 6 to 1), suggests that FA 3 was deposited in a lower to middle shoreface environment (MacEachern & Pemberton 1992). The absence of pebbles and shell beds support these shoreface settings. The amalgamation of sandstone bodies suggests storm currents as the principal creator of the deposits, whereas an evidence of tidal influence was absent. During storm events, the sand was remobilised and transported offshore (especially into FA 2). Given the relatively highly bioturbated nature of the beds, the storms probably represented low frequency, but moderate to potentially high-energy events within a lower to middle shoreface setting (Pemberton et al. 2001). The deposits of FA 3 were interpreted to reflect mostly the low-energy shoreface condition (MacEachern & Pemberton 1992).

Sedimentological evidence suggests that the Upper Cretaceous deposits of the KF were influenced by storm activity. It might have been connected to sea-level transgression reaching its maximum. A shoreline retreat due to erosion would have been significant and remobilization of sediments in the form of tempestites probably occurred (Baniak et al. 2013). The paucity of the upper shoreface deposits in FA 3 might be connected with rapid shoreface retreat and storm activity; however, the common presence of highly bioturbated sediments suggests that the frequency of storms would have been low to moderate (MacEachern & Pemberton 1992; Baniak et al. 2013).

Gamma-ray spectral analysis

Deposits of the KF reveal varied gamma ray spectra. Concentrations of K for the FA 1 samples were mostly below the detection limit (i.e., 0.2 %) and reached a maximum of 1 %. The concentration of K for the FA 2 samples varied from 0.7 % to 1.2 % and for the FA3 samples from 0.9 % to 1.3 %. Concentrations of U for the FA 1 samples varied from 0.3 ppm to 1.3 ppm, although in a few cases, they were below the detection limit (i.e., 0.3 ppm). Similarly, concentrations of U for the FA 2 samples varied from 0.7 to 1.3 ppm, and in a few cases, they were below the detection limit. Concentrations of U in samples of FA 3 were always below the detection limit. Concentrations of Th for the FA 1 samples varied from 1 to 7.8 ppm (average; AVG 4.2 ppm). Concentrations of Th for the FA 2 samples varied from 2 to 7.6 ppm (AVG 4.8 ppm), and for FA3 varied from 3.4 to 7.1 ppm (AVG 5.3 ppm). Evaluations of concentrations of radioactive elements, according to Hasseblo (1996), indicate their presence can be evaluated mostly as low (especially U and K), and less commonly as moderate to high (Th). The values of both Th/K and Th/U ratios ranged significantly from low to high values, but high values were more typical. Due to some missing values in concentrations of U and K, it was always not possible to estimate the ratios. The value of total radioactivity or SGR is similarly relatively low for all recognised FA.

Interpretation: Generally low concentrations of radioactive elements are interpreted as a signal of the high carbonate material content. Varied concentrations of radioactive elements coincide with the results of facies analyses/lithology (see Rider 1991). Relatively higher concentrations of K and Th, as well as lower concentrations of U are connected with FA 3. Conversely, the relatively higher concentrations of U and lower concentrations of Th and K correspond to FA 1. Such results can be interpreted as a signal of the generally varied lithology of individual FA and an important role of post-depositional processes. The most varied concentrations of K, are connected with the role of sand and silt detrital components. Low concentrations of K for pelitic FA 1 deposits point to their lower illite (and glauconite) content. Increased K content in FA 2 and FA 3 may reflect the increasing presence of glauconite. Generally low concentrations of U are related to the post-depositional condition and its leaching. The variations of Th concentrations for the recognised FA are explained as a signal of terrestrial minerals in clastics and low concentrations of kaolinites in pelites. According to Doveton & Merriam (2004), the Th/K ratio can be applied to the recognition of clay minerals and the distinction of micas and K-feldspars. Similar values of the Th/K ratio and its high variability implied high variations in both unstable and stable minerals in the samples studied. This result reveals high differences in the mineral and chemical maturities of the studied samples.

The U versus Th plot (Fig. 8A) indicates that the majority of the samples are located below the separation line, so the authigenic enrichment of U is missing and might signalize

that the samples have no significant organic matter (Myers & Wignall 1987).

The Th/U ratio has also proved to be useful in the recognition of geochemical facies or as an indicator of the redox-potential (Myers & Wignall 1987; Doveton 1991) or even the depositional environment (Adams & Weaver 1958). The cross plot of Th/K versus Th/U ratios is presented in Fig. 8B. Higher values of both Th/U and Th/K ratios for samples from FA 1 than from FA 2 are explained as evidence of oxidic conditions during their deposition of pelites and post-depositional leaching for heterolites. Generally high Th/U ratio of marine deposits of KF probably signalise the role of post-depositional processes on U concentrations. Deposits reveal a character of mixed clay structures (Ruffell & Worden 2000).

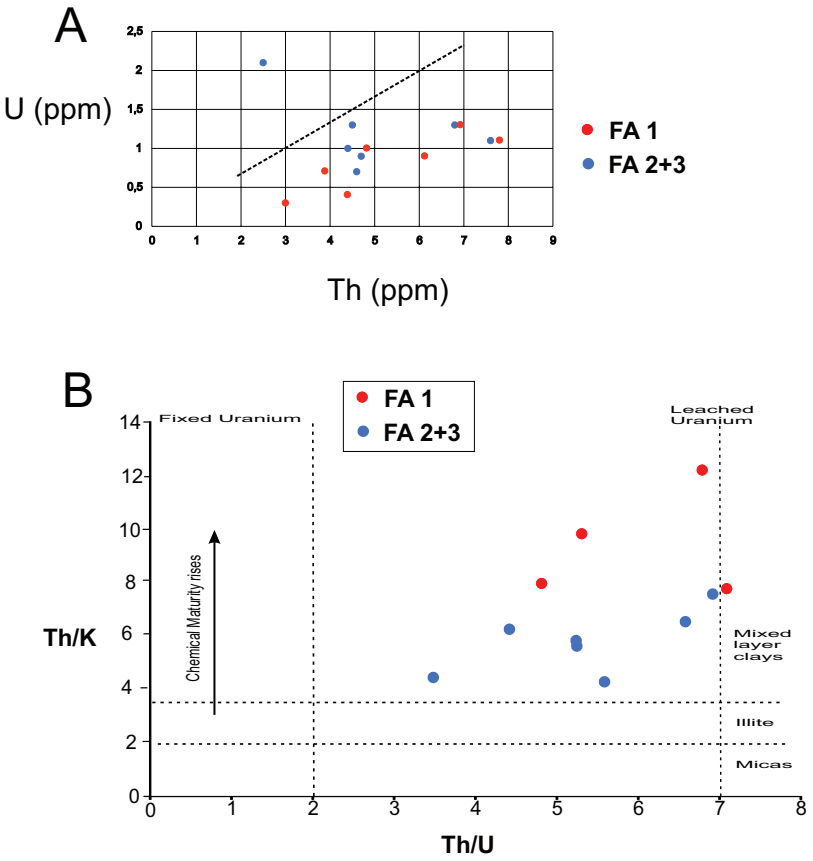

Fig. 8. Results of Gamma-ray spectral analysis. **A** — Crossplot of U versus Th with a discrimination line Th/U=2. **B** — Crossplot of Th/K versus Th/U ratios with types of clays.

Heavy mineral studies

Heavy mineral assemblage

Heavy mineral studies are commonly used for evaluation of the provenance, condition of weathering, transport, deposition, and diagenesis. Studying heavy mineral association was combined with ZTR index discrimination (zircon+tourmaline+rutile), which reflects of the mineralogical "maturity" (Hubert 1962; Morton & Hallsworth 1994), especially in cases of similar supposed sources.

Staurolite (25.5 %) and garnet (23.6 %) dominate in the heavy mineral spectra, followed by kyanite (13.3 %), and significantly less common are zircon (7 %), rutile (6.72 %), and tourmaline (5.7 %). Apatite (4.2 %), epidote (4.2 %), amphibole (3 %), spinel (1.2 %), and andalusite (0.6 %) represent rare heavy minerals. The value of the ZTR reaches 19.4 %.

Interpretation: The significant staurolite and kyanite content indicates a source of Al-rich metapelites of upper greenschist- to amphibolite facies (Bucher & Frey 1994). The dominant presence of garnet confirms the significant role of metamorphic complexes (crystalline schists) in the source area. Zircon, tourmaline, and rutile are common in acidic to intermediate magmatic rocks, and similarly in selected metamorphic rocks (von Eynatten & Gaupp 1999). The relatively low value of the ZTR index signals a limited role of redeposition from older clastic deposits. The dominant source of rutile is commonly placed into medium to highly metamorphosed metapelites, or metamafites (Force 1980), or pegmatites (Zack et al. 2004a, b). Apatite is a typical accessory mineral of the most magmatic and metamorphic rocks. Rare occurrences of epidote point to low-grade metamorphic rocks and exceptional chromite to basic-ultrabasic magmatic rocks. The lower quantity of low-stable heavy minerals (apatite, amphibole, epidote, andalusite, etc.), points to a relatively intense weathering in the source area, formed by both crystalline schists and magmatic rocks (a mature continental crust).

Garnet

The chemistry of detrital garnet is used widely for the more detailed determination of source rocks). Nine garnet types were recognised in the studied deposits and Table 2 shows the relative abundance of these types. The results of the analyses reveal the dominance (38.7 %) of almandine–pyropes (pyrope/PRP 70–73 %, almandine/ALM 15–18 %, grossular/GRS 4–5 %, spessartine/SPS 1–3 %, andradite/ADR 1–2 %) as well as pyrope–almandines (22.6 %) (ALM 42–84 %, PRP 11–47 %, GRS 0–9 %, SPS 1–9 %, ADR 1–3 %) in the garnet type spectra.

Multivariate statistical analysis of garnet chemistry according to Tolosana-Delgado et al. (2018) recognises four sources of garnet (see Fig. 9A, B). The strong predominant source was from ultramafic rocks (70.6 %). Garnets from amphibolite metamorfic facies (28.4 %) or from granulite metamorfic facies (14.7 %) were less common. The role of garnets from igneous rocks (7.8 %) was minor and eclogite metamorfic facies was not recognised as a source.

Several ternary discrimination diagrams were utilised for a more detailed identification of the primary source of garnet (Fig. 9C, D). The diagram PRP–ALM+SPS–GRS (Mange & Morton 2007) in Fig. 8C reflects the most important role (35.2 %) of garnets from ultramafic rocks (e.g., pyroxenites, peridotites); less common are garnets from high-grade granulite facies metasediments or intermediate to felsic igneous rocks (both 18.5 %) or garnets from high-grade mafic rocks (16.7 %). Garnets from amphibolite-facies metasedimentary rocks (11.1 %) were even less common. Diagram PRP–ALM–GRS (Aubrecht et al. 2009) in Fig. 8D indicates the dominant (35.2 %) primary source of garnets is from ultramafic rocks (pyroxenites, peridotites) and felsic and intermediate granulites (27.8 %). Both garnets from gneisses metamorphosed under amphibolite facies conditions (22.2 %) and garnets from gneisses and amphibolites metamorphosed in conditions transitional to granulite and amphibolite metamorphic facies (14.8 %) were less common.

Table 2: Recognised garnet types in the deposits of the Klement Formation.

Garnet type	Jurassic		Cretaceous
	Gresten Fm. (%)	Nikolčice Fm. (%)	**Klement Fm.** (%)
ALM$_{48–84}$**PRP**$_{11–47}$GRS$_{0–9}$SPS$_{1–9}$ADR$_{1–3}$	**71.2**	**82.5**	**22.6**
ALM$_{54–79}$**GRS**$_{11–30}$PRP$_{0–9}$SPS$_{1–9}$ADR$_{1–7}$	6.8	1.9	8.1
ALM$_{74–89}$GRS$_{0–9}$PRP$_{3–9}$SPS$_{1–9}$ADR$_{0–2}$	3.4	3.8	8.1
ALM$_{51–78}$**GRS**$_{12–32}$**PRP**$_{10–19}$SPS$_{1–4}$ADR$_{1–2}$	1.7	1.9	8.1
ALM$_{42–76}$**SPS**$_{11–40}$**PRP**$_{11–16}$GRS$_{1–4}$ADR$_{0–2}$	5.1	–	8.1
ALM$_{43–68}$**GRS**$_{14–33}$**SPS**$_{11–19}$PRP$_{1–7}$ADR$_{1–3}$	5.1	–	–
ALM$_{48–81}$**SPS**$_{11–40}$Prp$_{3–10}$ADR$_{0–2}$GRS$_{0–8}$	3.4	3.8	–
ALM$_{40–69}$**PRP**$_{16–40}$**GRS**$_{11–15}$SPS$_{0–8}$ADR$_{0–1}$ AV$_{0–1}$	–	1	–
ALM$_{63–73}$ **PRP**$_{14–22}$**SPS**$_{11}$GRS$_{1–2}$ ADR$_{21}$	–	3.8	1.6
ALM$_{48–55}$**SPS**$_{23–26}$**GRS**$_{14–20}$ PRP$_{2–9}$ADR$_{1–3}$	–	–	3.2
PRP$_{70–73}$**ALM**$_{15–18}$GRS$_4$SPS$_{1–3}$ADR$_{2–5}$	1.7	–	**38.7**
AV$_{53}$**PRP**$_{27}$**ALM**$_{18}$	1.7	–	–
SPS$_{39}$**ALM**$_{35}$**GRS**$_{13}$PRP$_5$ADR$_8$	–	1	–
ADR$_{49–54}$ **PRP**$_{41–44}$ALM$_4$SPS$_1$	–	–	1.6

Almandine–pyropes and pyrope–almandines have been derived from metamorphosed ultrabasic rocks. The almandine garnets point to primary sources from gneisses and mica schists. A wide variety of garnet types is recognised, despite limited amount of analyses; this indirectly points to the redeposition and recycling of material from older deposits. Specifically, the data can be compared with the results from the Moravian–Silesian Paleozoic deposits, where the strong dominance of pyrope–almandines (close to 80 %) is typical for its younger part, i.e., the Myslejovice Formation (Otava et al. 2000; Čopjaková et al. 2002). The high-pyrope garnets are known to be abundant in the Mesozoic sediments of the Outer Western Carpathians (Pieniny Klippen Belt) (Aubrecht & Méres 2000; Aubrecht et al. 2009; Méres et al. 2012).

Rutile

Rutile represents one of the most stable heavy minerals, so it is often used for provenance analyses (Force 1980; Zack et al. 2004a, b; Triebold et al. 2007).

The concentrations of the main diagnostic elements (Fe, Nb, Cr and Zr) vary significantly in the studied samples. The Fe content shows that 56 % of the rutile analysed originated from metamorphic rocks. The concentrations of Nb ranged between 137 and 5572 ppm (the average is 1362 ppm); concentrations of Cr varied between 10 and 2226 ppm (the average is 658 ppm); and the concentrations of Zr ranged from 10 to 8244 ppm (with an average 812 ppm) and the absolute majority (72 %) of log(Cr/Nb) values was negative. A majority (64.3 %) of metamorphic rutile from the KF originates from metapelites (e.g., mica-schist, paragneiss, felsic granulite), and a minority (36.7 %) originating from metamafic rocks (eclogite, basic granulite), according to the grouping by Zack et al. (2004a, b) and Triebold et al. (2007). According to the diagnostic criteria of Triebold et al. (2012), 92.9 % of the metamorphic rutile originates from metapelites and only 7.1 % from metamafic rocks. A discrimination plot of Cr vs. Nb is shown in Fig. 10.

Zr-in-rutile thermometry was applied on metapelitic rutile only (see Zack et al. 2004a, b; Meinhold et al. 2008). The results indicate that the majority of metapelitic rutile originates from granulite metamorphic facies or possibly amphibole/eclogite facies. Sources from such highly metamorphosed crystalline indirectly point to advanced stages of erosion in the source area.

Zircon

Zircon is a very stable mineral used for evaluation of the source rocks, role of recycling, relative age, conditions of the parental magma formation, and erosional rate, etc. (Poldervaart 1950; Zimmerle 1979; Mader 1980; Pupin 1980, 1985; Winter 1981; Finger & Haunschmid 1988; Lihou & Mange-Rajetzky 1996).

Of the zircon varieties, euhedral zircons represent 9.8 %, subhedral zircons form 26.8 %, subrounded are at 59.4 %, and well rounded represent 3.9 %. Crystal faces were identified at 59.9 % of zircon grains. The fracturing of zircon grains affected approximately one-third (35.2 %) of the grain spectra. Grains fractured nearly parallel to the c-axis were significantly more common (96.5 %) than grains fractured perpendicular to the c-axis (3.5 %). Cracks were recognised in the majority of grains (75.9 %). Pale zircon (50.6 %) dominated, colourless zircon (37.8 %), brown zircon (9.9 %), and opaque zircon (1.7 %). The proportion of zoned zircons is lower, reaching only 7.4 %, similar to zircons with older cores (5.6 %). Inclusions were recognised in 94.4 % of the studied grains.

The average value of the elongation of the zircon (the relationship between the length and width of crystals) is 2.2.

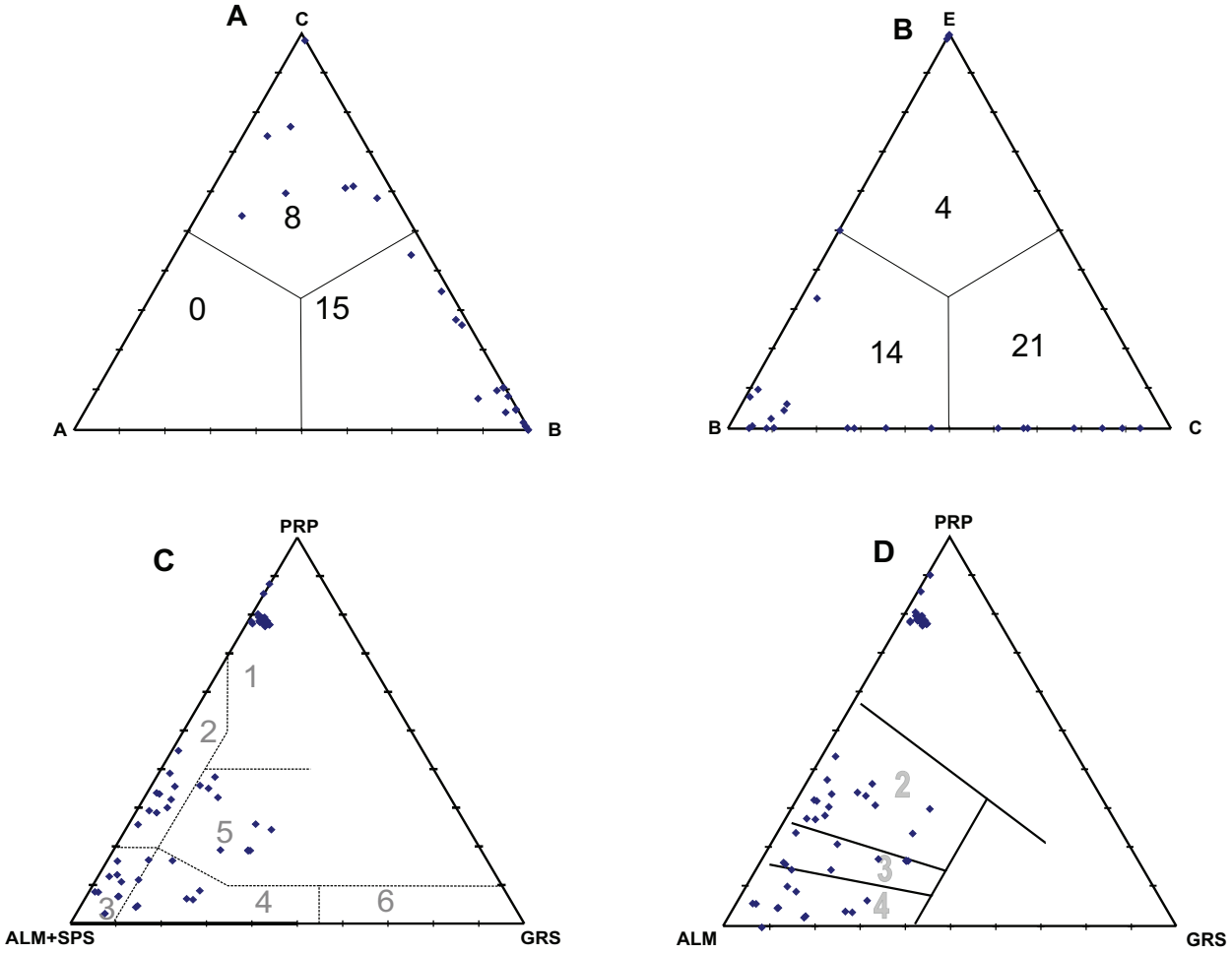

Fig. 9. Ternary diagrams of the chemistry of detrital garnets (ALM – almandine, GRS – grossular, PRP – pyrope, SPS – spessartine). **A** — Ternary diagram based on multivariate analysis according to Tolsana-Delgado et al. (2018) (A – eclogite facies, B – amphibolite facies, C – granulite facies); **B** — Ternary diagram based on multivariate analysis according to Tolsana-Delgado et al. (2018) (B – amphibolite facies, C – granulite facies, E – igneous rocks). Numbers within the diagrams refer to number of analyses in the discrimination field. **C** — Discrimination diagram according to Mange & Morton (2007) (1 – pyroxenes and peridotites, 2 – high-grade granulite facies metasediments and intermediate felsic igneous rocks, 3 – intermediate to felsic igneous rocks, 4 – amphibolite facies metasedimentary rocks); **D** — Discrimination diagram according to Aubrecht et al. (2009) (1 – pyroxenes and peridotites, 2 – felsic and intermediate granulites, 3 – gneisses and amphibolites metamorphosed under pressure and temperature conditions transitional to granulite and amphibolite facies metamorphism, 4 – gneisses metamorphosed under amphibolite facies conditions).

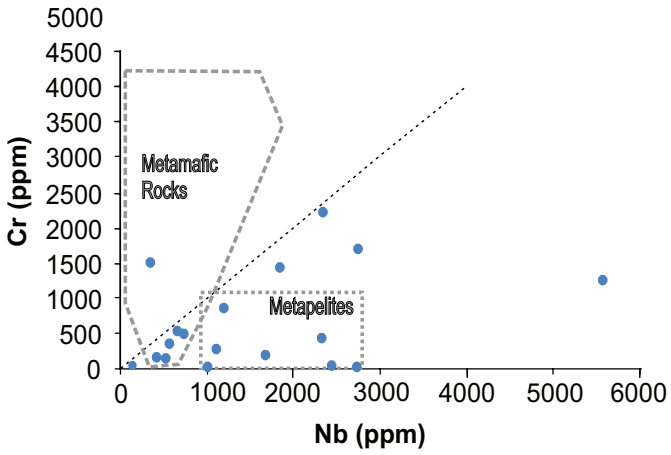

Fig. 10. Discrimination plot of Cr vs. Nb of investigated rutiles. Discrimination plot according to Zack et al. (2004b).

Zircon with an elongation above 2.0 is more common (56 %) than zircon with elongation below 2.0 (44 %). Zircon with an elongation of more than 3 represented only 6 %. Such zircon is supposed to reflect volcanic origins and/or limited transport (Zimmerle 1979). The maximum elongation was 4, however, the prism of the columnar zircon crystals were commonly broken. The high portion of broken zircon points primarily to a higher content of zircon with higher elongation values.

The study of zircon typology mainly points to crustal origin of paternal magma (Pupin 1980, 1985). The most

common were the typological subtypes S18 (28.8 %), S17 (21.6 %), and S13 (10.7 %). The presence of subtypes S20, S14, S24, S12, and S16 was less common and varied between 5.4 % and 7.2 %. Further subtypes, i.e., S11, S18, S19, S23, and S25 were relatively rare (at less than 2 %). This can be interpreted due to the dominant source of magma of calc-alkaline affinity (Pupin 1980).

U–Pb dating of zircon

The Th/U ratios of zircon grains (103 analysed grains, sample from the well Mikulov 5) can be used to reflect the origin of the zircon, where high Th/U ratios of greater than 0.3 and low ratios of lower than 0.1 generally indicate igneous and metamorphic origins, respectively (Möller et al. 2003). In this study, the Th/U ratios of the zircon grains range from 0.01 to 1.34 (Fig. 11). Only 3 grains (2.9 %), however, have values less than 0.1. Most values (84.3 %) are over 0.3, which supports the notion they originate from igneous rocks.

Detrital zircon age spectra is presented in Fig. 12. The largest zircon population is from the Paleozoic (n=61/59.3 %), i.e., Cambrian n=10/9.7 % (ages between 490.4 Ma and 539.0 Ma); Ordovician n=6/5.8 % (ages between 451.1 Ma and 473.6 Ma); Silurian n=1/1 % (age 424.0 Ma); Devonian n=19/18.5 % (ages between 359.5 Ma and 403.9 Ma) and Carboniferous n=25/24.3 % (ages between 310.1 Ma and 358.8 Ma). The population of Carboniferous zircons is definitively dominated by Lower Carboniferous grains, which are mostly Tournasian (n=16) accompanied by Visean grains (n=4). Upper Carboniferous zircon is significantly less common, as either Bashkirian (n=4) or Moscovisan (n=1). Younger zircon than 310.1 Ma is missing. Similarly, the population of Devonian zircon is dominated by the upper Devonian being mostly Famenian (n=14) or Frasnian (n=4). Lower Devonian zircon (ems) is exceptional (n=1) and Middle Devonian zircon is missing, which confirms the key role of Variscan units in the source area.

Proterozoic zircons form 39.8 % and Neoproterozoic zircons (with ages between 542.4 Ma and 951.4 Ma) are dominant (33.0 %); it is less commonly Tonian (1 %) or Cryogenian (6.8 %), and mostly Ediacarian (25.2 %). It signalises the presence of Cadomian units in the source area. Paleoproterozoic zircons (with ages between 1737.8 Ma and 2322.5 Ma) represent 3.9 % and Mesoproterozic zircons (with ages between 1146.9 Ma and 1498.7 Ma) represent 2.9 % of the zircon spectra. The oldest zircon is Archean in age (1 %, with age 3232.9 Ma). These may represent inherited zircon cores based on CL images.

Palynological study

In the assemblages, the following species prevail: *Achomosphaera triangulata, Circulodinium distinctum, Exochosphaeridium muelleri, Hystrichodinium pulchrum, Palaeohystrichophora infusorioides, Spiniferites ramosus, Odontochitina operculata, Oligosphaeridium complex, Palaeoperidinium cretaceum, Pervosphaeridium pseudhystrichodinium, Protoellipsodinium spinosum*, and others. The results of the palynological study are presented in Figs. 13 and 14 and Tables 3 and 4.

The sample provided rich dinoflagellate cyst assemblage typical of the late Albian. *Palaeohystrichophora infusorioides* first appeared in the uppermost Albian (Stoliczkaia dispar Ammonite zone) in France (Tocher & Jarvis 1987). According to the dinoflagellate events listed by Williams et al. (2004), for the northern mid-latitudes, the FO of *P. infusorioides* defines an age of 99.85 Ma, using the time-scale of Gradstein et al. (1995). This corresponds again to a Late Albian age.

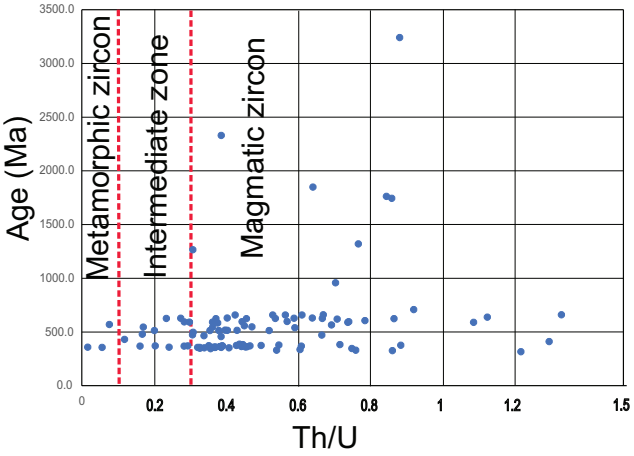

Fig. 11. The Th/U ratios of zircon grains of the Klement Formation.

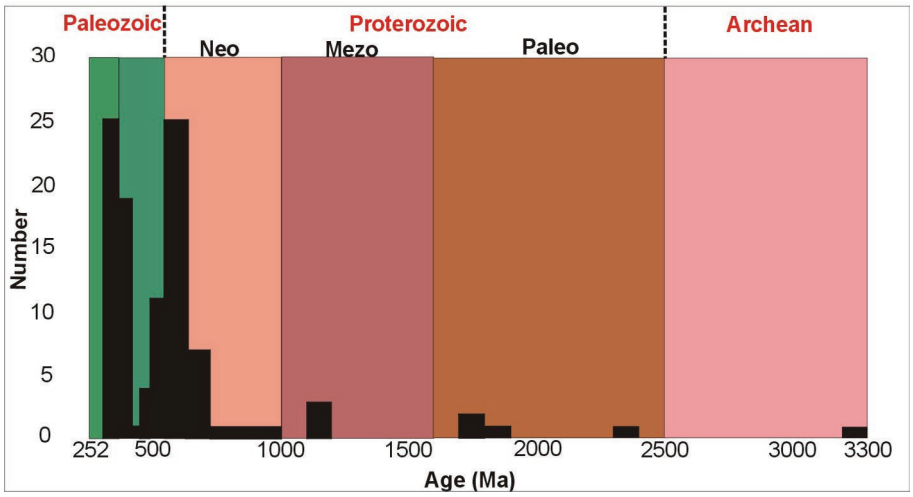

Fig. 12. Detrital zircon age spectra of the Klement Formation.

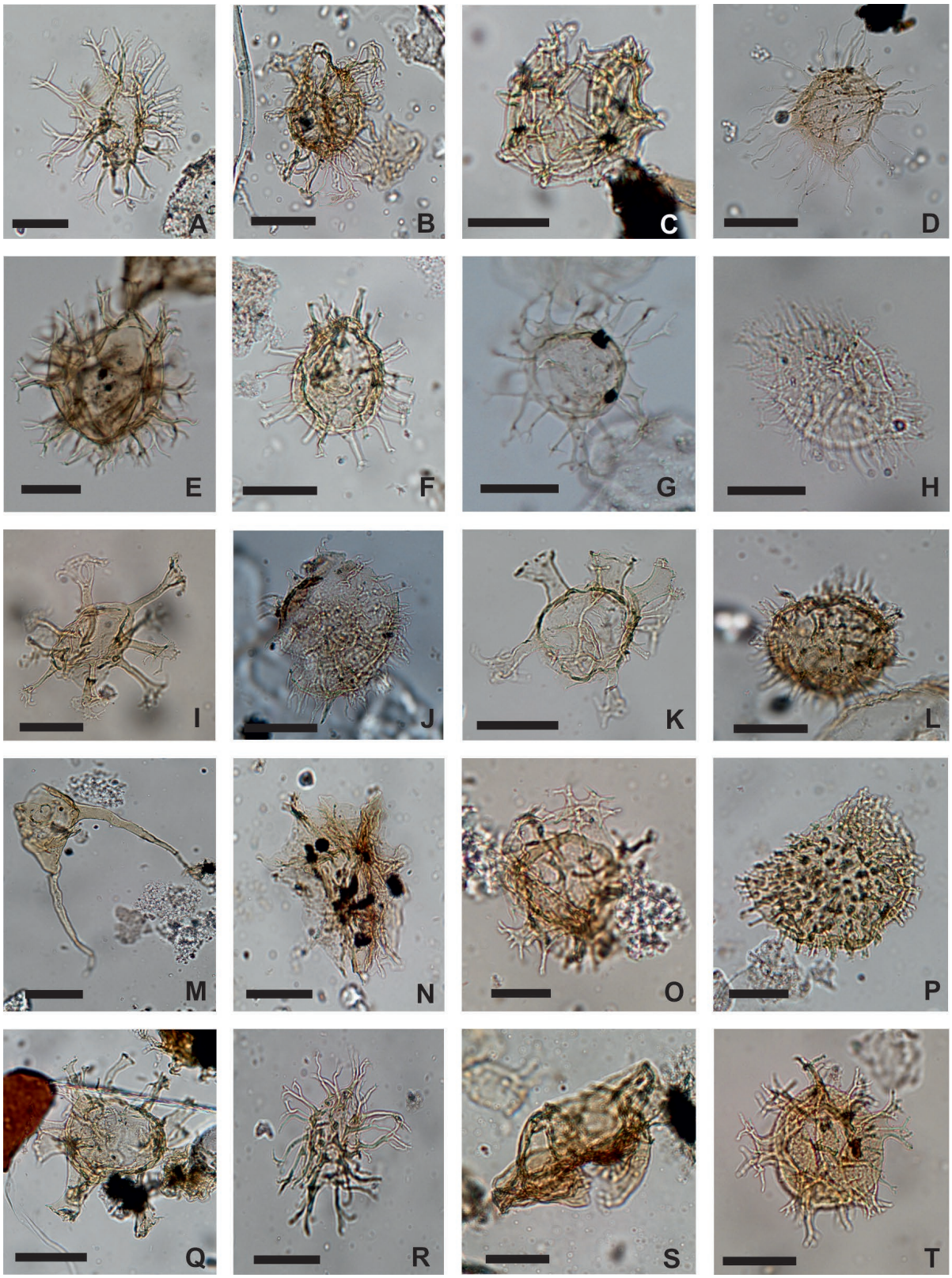

Fig. 13. Selected examples of dinoflagelates recognised in the deposits of the Klement Formation. **A** — *Achomosphaera triangulata*; **B** — *Hystrichosphaerina schindewolfii*; **C** — *Pterodinium cingulatum*; **D** — *Hystrichodinium pulchrum*; **E** — *Spiniferites ramosus*; **F** — *Kiokansium polypes*; **G** — *Achomosphaeara ramulifera*; **H** — *Palaeohystrichophora infusorioides*; **I** — *Oligosphaeridium complex*; **J** — *Pervosphaeridium truncatum*; **K** — *Callaiosphaeridium asymmetricum*; **L** — *Pervosphaeridium pseudhystrichodinium*; **M** — *Odontochitina operculata*; **N** — *Atopodinium perforatum*; **O** — *Hystrichostrogylon membraniphorum*; **P** — *Circulodinium distinctum*; **Q** — *Florentinia stellata*; **R** — *Surculosphaeridium longifurcatum*; **S** — *Stephodinium coronatum*; **T** — *Spiniferites ramosus reticulatus*.

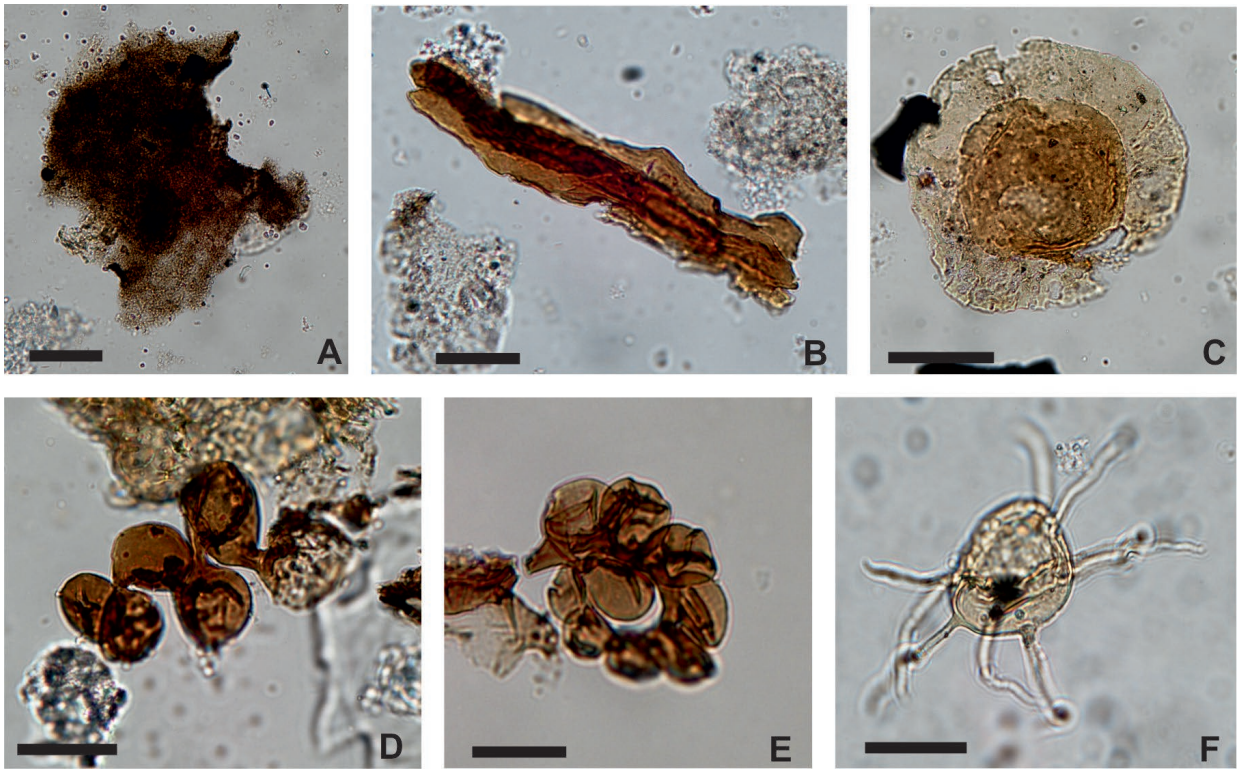

Fig. 14. Selected examples of dinoflagelates recognised in the deposits of the Klement Formation. **A** — Amorphous organic matter (AOM); **B** — Brown phytoclast; **C** — *Pterospermella* sp.; **D, E** — Foraminifera test linings; **F** — Acritarch *Veryhachium.*

Achomosphaera ramulifera	5
Achomosphaera triangulata	5
Atopodinium perforatum	1
Callaiosphaeridium asymmetricum	1
Circulodinium distinctum	14
Circulodinium vermiculatum	1
Coronifera oceanica	1
Exochosphaeridium muelleri	24
Exochosphaeridium truncatum	1
Florentinia stellata	2
Heterosphaeridium sp.	7
Hystrichodinium pulchrum	15
Hystrichosphaerina schindewolfii	1
Hystrichostrogylon membraniphorum	1
Kiokansium polypes	5
Kleithriasphaeridium eoinodes	1
Odontochitina operculata	8
Oligosphaeridium complex	8
Palaeohystrichophora infusorioides	19
Palaeoperidinium cretaceum	4
Pervosphaeridium pseudhystrichodinium	4
Pervosphaeridium truncatum	1
Polysphaeridium sp.	5
Protoellipsodinium spinosum	8
Pterodinium cingulatum	1
Spiniferites ramosus	19
Spiniferites ramosus.reticulatus	2
Stephodinium coronatum	1
Surculosphaeridium longifurcatum	3
Systematophora cretacea	1

Table 3: Dinoflagellate cysts association in the samples of Klement Fm. from the borehole Mikulov 5.

According to *Protoellipsodinium spinosum and Systematophora cretacea* the stratum is not younger than late Albian. The LO of *P. spinosum* is, according to Costa & Davey (1992) known in the late Albian. It is further supported by the presence of *Pervosphaeridium truncatum*, whose range, according to Costa & Davey (1992), is only the late Albian.

It is a diversified and, above all, well-preserved community, in which marine elements (dinoflagellates, foraminifera linings) significantly predominate over terrestrial counterparts (pollen and spores).

The studied palynological assemblages are dominated by dinoflagellate cysts (32 %). Representatives of acritarchs are rare, representatives of the genus *Veryhachium* are rarely found. Prasinophyte algae are rare, only *Pterospermella* sp. The spore-pollen assemblage is not well preserved. A strong terrestrial influence is documented by numerous woody phytoclasts ranging from dark brown to black in colour

A relatively well-preserved assemblage is dominated by the dinocyst species *Palaeohystrichophora infusorioides.* Other dinoflagellate cysts constitute a mixture of the neritic species *Oligosphaeridium complex, Surculosphaeridium longifurcatum, Florentinia stellata, Hystrichodinium pulchrum*, and shallow-marine elements such as *Odontochitina operculata* (Leereveld 1995; Skupien et al. 2013). Due to the dominance

Table 4: Percentage content of organic particles in the samples of Klement Fm. from the borehole Mikulov 5.

Group	Constituents		%
Phytoclasts	Opaque	Lath	15.80
		Equidimensional	17.00
	Translucent	Brown particle	7.21
		Light brown and yelow	8.24
		Cuticle	9.00
AOM	AOM		1.66
Palynomorphs	Spores		2.04
	Pollen		1.00
	Dinoflagellate cysts		32.45
	Foraminifera test linings		4.56
	Acritarchs		1.00

of *Palaeohystrichophora infusorioides*, and the presence of chitinous foraminiferal linings, a shallow marine environment is assumed. The influence of deeper-sea conditions is evidenced by the presence of *Pterodinium cingulatum* (Lister & Batten 1988; Leereveld 1995).

Thermal maturity

The Rock-Eval pyrolysis allowed the evaluation of the hydrocarbon potential, organic matter type and thermal maturity level within the studied data set. The organic carbon content (TOC) in the samples varied from 0.1 % to 0.4 %. The bound hydrocarbons (S2) ranged from 0.1 to 0.2 mgHC/g rock. Based on the TOC contents (Table 5) all samples displayed a "poor" quality (TOC <0.5 %) to generate hydrocarbons. The studied samples also had low HI values, from 44 to 106 mg HC/g TOC with an oxygen index (OI) from 39 to 195 mg CO_2/g TOC. By plotting the OI versus HI (Fig. 15) as proposed by Peters et al. (2005), the analyzed samples represent type III kerogen, which is derived from higher plants and is gas prone.

This finding is in agreement with published results (Zahajská et al. 2024) where coastal halophytic vegetation growing in the BCB was described. In the depositional environment of the shallow sea, terrestrial organic matter debris is also to be assumed, which corresponds to kerogen III.

The maximum pyrolytic temperature (Tmax) varies from 417 to 427 °C. According to Tmax values and production index (PI), the samples from the KF belong to immature range (Table 5).

Discussion

Albian age of the studied deposits of the KF was determined based on palynological assemblages. The studied Albian deposits are connected to the "initial" transgression (Albian–Lower Cenomanian) onto the Bohemian Massif (Čech & Valečka 1991). Svobodová (1992) and Svobodová & Brenner (1999) suggested the possible Albian Age for the lowermost paleovalley fill in the Blansko Graben (eastern part of the BCB). It is generally supposed that the earliest infill of the BCB is represented by a diverse suite of fluvial to shallow-marine facies of Cenomanian (Uličný et al. 2009b). The drainage of the entire Bohemian Basin toward the Tethys was suggested by Klein et al. (1979) and Voigt (1998). However, Uličný et al. (2009b) recognised several local paleodrainage systems which developed in the BCB during the Cenomanian; and reported on the role of the Nové Město–Holice Paleohigh (trending roughly north-northeastward) as a major drainage divide. This paleohigh separated the eastern part of the BCB, which drained toward the southeast Tethyan margin; the rest of the basin drained towards the Boreal paleogeographic realm, until its final submergence during the late Cenomanian to early Turonian. The locations and directions of paleovalleys were controlled by the positions of the inherited Variscan basement fault zones.

Systems that drained the Bohemian Massif toward the Tethyan province, followed the Železné Hory Fault Zone to the west and Orlice Graben faults to the north (Uličný et al. 2009b). Several source areas for the deposits of these drainage systems have been reported. Simplified map of regional geological units which might served as possible source areas is presented in Fig. 16A. According to Mitchel et al. (2010) the Orlice–Žďár Sub-basin in the south-eastern part of the BCB

Table 5: Bulk geochemical data of Rock-Eval and TOC analysis with calculated parameters from Cretaceous sediments.

Borehole ID	Lithology	Depth (m)	TOC (wt. %)	S_1 (mg HC/g)	S_2 (mg HC/g)	S3 (mg CO_2/g rock)	T_{max} (°C)	HI	OI	PI
NM 2	siltstone	2220	0.2	0.10	0.15	0.21	*422*	73	103	0.41
NM 3	siltstone	2232	0.1	0.04	0.05	0.18	*	48	171	0.44
Pavlov 1	siltstone	1580	0.3	0.07	0.16	0.26	*417*	59	96	0.29
Sedlec 1	siltstone	3526	0.1	0.03	0.09	0.16	*422*	129	129	0.25
Strachotín 2	siltstone	1795	0.1	0.03	0.07	0.12	*	195	195	0.32
Sedlec 1	siltstone	3566	0.4	0.01	0.18	0.16	*427*	39	39	2.94

TOC: Total organic Carbon, wt. %.
S1: Volatile hydrocarbon (HC) content, mg HC/g rock.
S2: residual petroleum potential; mg HC/g rock.
S3 : CO_2 from decomposition of the organic matter; mg CO_2/g rock
*not representative data
Tmax: Temperature at maximum of S2 peak.
HI: Hydrogen Index = S2*100/TOC, mg HC/g TOC.
OI: Oxygen Index = S3*100/TOC, mg CO_2/g TOC.
PI: production index

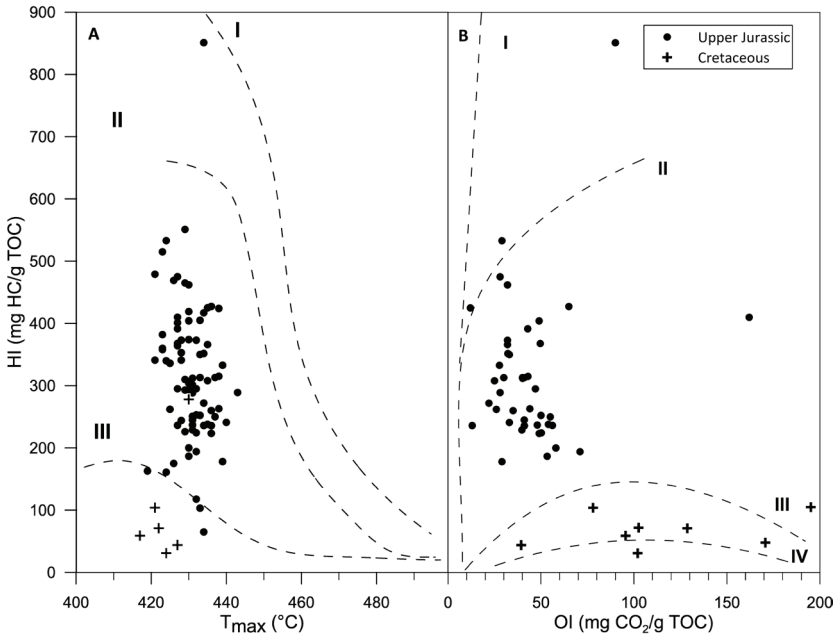

Fig. 15. A — The cross-plot of hydrogen index (HI) versus Rock-Eval temperature Tmax, with maturation pathways for kerogen types for Cretaceous sediments. **B** — Plots of Hydrogen Index (HI) versus Oxygen index (OI) classified the kerogen as type III. Kerogen type maturation paths according to Espitalié et al. (1985).

received material from uplifted basement blocks south of the Labe–Železné Hory Fault Zone. Frejková & Vajdík (1974) and Frejková (1984) located a significant portion of clastic material from the Orlice Basin Permian strata initially, whereas the provenance from metamorphosed units located further northwest and northeast, especially the Zábřeh Metamorphic Complex, which dominates in the higher portion of succession.

The provenance from the eastern margin of the Bohemian Massif is supposed and some potential source areas of the deposits of the KF can be evaluated after comparison with published data from the nearby basement rocks forming adjacent areas (see Fig. 16B). The principal and proximal source is located in the geological unit of the Moravo–Silesian Zone (Brunovistulicum) which composes the crystalline basement of the KF. Ediacarian zircons in particular could be sourced from this unit. The very low Tonian zircon content excludes the western metabazalt subzone of the metabazite zone of the Brno Massif as an important source (Finger et al. 2000; Hanžl et al. 2019). This source is further implicated by the high content of garnets sourced from ultrabasic rocks, which also constitute this subzone. The Cryogenian age of the metadiorite subzone (655–650 Ma) was recognised by Hanžl et al. (2019). The zircons from the Late Ediacarian to the Lower Paleozoic sedimentary cover of Brunovistulicum provided a broad spectrum of ages, predominantly the Ediacarian, and some zircons from the Tonian to Cryogenian Age (740–704 Ma) up to Mesoproterozoic and Archean (2.8–3.4 Ga) (Habryn et al. 2020; Żelaźniewicz & Fanning 2020). Similarly, detritic zircons from metasedimentary rocks of the Moravo–Silesian Zone are mostly Ediacarian in age (570–550 Ma) with some Archean-to-Proterozoic zircons (2.6–1 Ga) (Jastrzębski et al. 2021; Soejono et al. 2022).

Slightly more distant probable sources can be traced to the more western geological units of the Bohemian Massif, ie., the Moravian and Moldanubian units. The Bittesch gneiss of the Moravian unit provides data of Ediacarian age (from 2.6 Ga to 2.0 Ga) (Friedl et al. 2004). An absolute majority (97.7 %) of Devonian and Carboniferous zircons can be compared with the data for the main group of Variscan to early post-Variscan intrusions (i.e. 310–380 Ma) (Cháb et al. 2020) which are located into the Central Moldanubian pluton. Similarly, Mesoproterozoic zircons could be compared with results from Dobra or Hauergraben orthogneisses from the Austrian part of the Moldanubian zone (Friedl et al. 2000, 2004; Lindner et al. 2020, 2021). Mesoproterozoic zircons are rare in granitic and metasedimentary rocks of the Brunovistulicum, similar to its late Ediacaran sedimentary cover (Żelaźniewicz et al. 2009; Habryn et al. 2020; Żelaźniewicz &Fanning 2020; Soejono et al. 2022).

Cambrian to Silurian zircons can be assigned to the Moldanubian unit or in even more distant sources, such as the Teplá–Barrandian or Lugicum units. They were possibly sourced from the Gföhl gneiss (488±6 Ma) in the Moldanubian unit (Friedl et al. 2004), felsic metavolcanic rocks in the Moldanubian Thrust Zone (575–498 Ma) (Jastrzębski et al. 2015), and the Letovice Complex (530 Ma) (Soejono et al. 2010). Cambro–Ordovician magmatism was documented as well from the Klodzko Metamorphic complex (500.4±3.1 Ma) by Mazur (2004).

Although the results of U–Pb dating of zircon allude to direct transport from crystalline rocks, the dominance of subrounded and rounded zircon grains indicates the role of redeposition and sedimentary recycling. Probable second-cycle sources from the syn-Variscan or post-Variscan sedimentary formations located in the units adjacent to the study area could be the rocks of the Moravo–Silesian Paleozoic deposits (Culm Facies) (see Xiao et al. 2024). However, the studied deposits of the KF reveal significantly higher evidence of Neoproterozoic zircons (33 %) compared to the Moravo–Silesian Paleozoic deposits (12–19 %), mostly due to the content of Carboniferous zircons (24 % versus 39–65 %). These findings did not support the significant role of zircon redeposition from the Moravo–Silesian Culm deposits for the KF.

Comparisons with clastic Jurassic deposits of Gresten and Nikolčice Formations (Nehyba & Opletal 2016, 2017) that fill the basal portion of the Dyje–Thaya depression reveal remarkable differences, particularly in the garnet spectra (see Table 2),

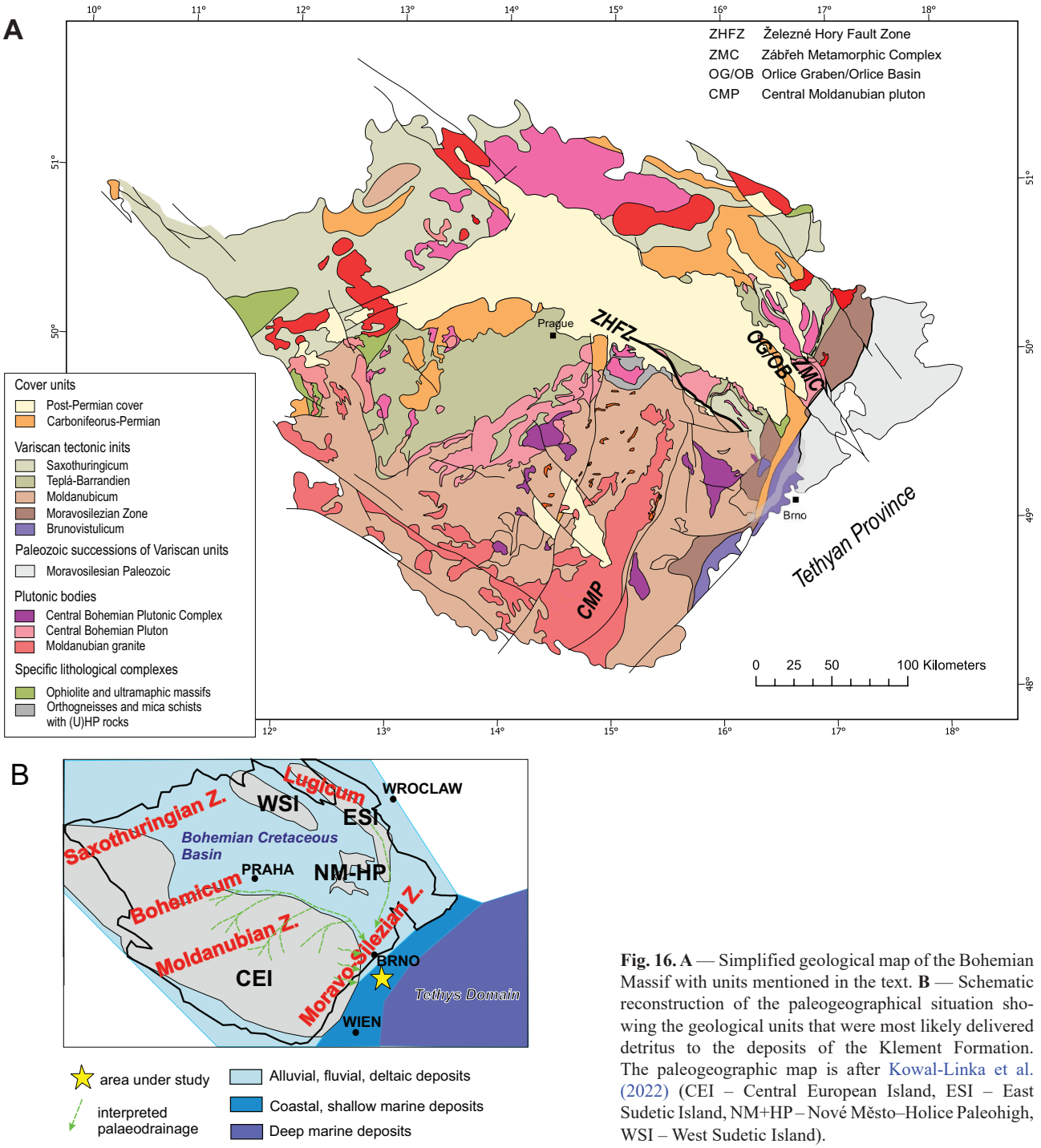

Fig. 16. A — Simplified geological map of the Bohemian Massif with units mentioned in the text. **B** — Schematic reconstruction of the paleogeographical situation showing the geological units that were most likely delivered detritus to the deposits of the Klement Formation. The paleogeographic map is after Kowal-Linka et al. (2022) (CEI – Central European Island, ESI – East Sudetic Island, NM+HP – Nové Město–Holice Paleohigh, WSI – West Sudetic Island).

heavy mineral assemblage, and zircon typology. Garnets from the KF provide significantly higher abundance of ultramafic rock sources and less evidence for sources from intermediate to felsic igneous rocks and gneisses metamorphosed under amphibolite facies conditions. The paleodrainage system developed on subaerial unconformity and the base of the KF represents a composite, polyhistory surface.

The basal unconformity of the BCB provides evidence of paleoweathering zones up to several tens of metres thick and significant paleorelief (Uličný et al. 2009b and references therein). This surface records a period of planation and intense weathering in the Bohemian Massif that lasted for much of the Mesozoic. Eliáš (1981) and Hanzlíková & Bosák (1977) supposed a comparable areal extent of the Jurassic (Callovian–Kimmeridgian) depositional episode as the one of the BCB. It is noteworthy that the subsurface extent of the Jurassic deposits on the eastern slopes of the Bohemian Massif is significantly larger than the extent of the Cretaceous counterparts (Pícha et al. 2006) due to significant Jurassic rifting. The identified differences in provenance are difficult to explain by

varied erosion levels due to successive exhumations of the source within the crystalline rocks of the Bohemian Massif; they exclude a marked Cretaceous erosion and redeposition of the clastic Jurassic deposits. We can suppose that significant reconstruction of the source area with different paleodrainage systems occurred.

Varied paleogeography of the studied Jurassic and Cretaceous depositional systems have been well documented through 3D seismic dataset interpretation (Figs. 3, 4, 5, 6). The basement of the Jurassic depositional system was initially (during the deposition of Gresten and Nikolčice Formations) dipping slightly southwestwardly with a quick dip increase during the main Jurassic rifting phase. The Upper Jurassic basin forms a more or less subhorizontal surface before the deposition of the Cretaceous sediments. The 3D seismic data interpreted the thicknesses of the KF which point to the different geometry of the basin. The thicknesses generally are increasing eastwards indicating a general increase in basin depth in this direction. The thickness dataset is unfortunately rather limited, as the seismic dataset does not allow for clear geological interpretation in its south-southeastern part as it is dipping steeply out of the reach of seismic data; this is also the case in its north-northwestern part where the original thickness is unclear due to subsequent erosion of Cretaceous sediments during the Neogene (Figs. 3, 4, 5, 6).

The source area of the clastic Jurassic deposits of Gresten and Nikolčice Formations can be localised into generally westward located paleo-highs formed by crystalline units of the Moldanubicum and the Moravian Zone, and the Moravo–Silesian Paleozoic deposits (Culm Facies) (Nehyba & Opletal 2016, 2017). On the other hand, the provenance of the KF is located in the northwest and north, especially in the Brno Massif. Moreover, the role of redeposition from the Moravo–Silesian Paleozoic deposits also significatly differs. The pre-Cenomanian erosion probably significantly restricted the extent of the Moravo–Silesian Paleozoic deposits on the eastern slopes of the Bohemian Massif.

All the studied samples have a comparable degree of thermal maturity; however, the current depth is significantly different. This can be seen in Fig. 17 where Cretaceous sediments of the same maturity are spread from 1580–3566 m with no depth trend. The underlying Jurassic Mikulov marls show a mild trend with depth in the Nové Mlýny 2 well, and a more visible depth trend in the Sedlec 1 well. Such observations can be considered proof that the sediments were buried to the maximum depths before the West Carpathian overthrust. Also, the original dip of the platform depositional system increases steeply in the southeastward direction due to flexural subsidence caused by the thickening of the thrust of the Western Carpathian Nappe System (Fig. 18).

Conclusions

Geologic interpretation of 3D seismic datasets and the sedimentological and provenance studis were combined with palynology and source rocks analyses of well cores to approximate the depositional environment, source area, thermal maturity, and source rock properties of the Klement Formation deposits (Upper Cretaceous). These autochthonous deposits cover the southeastern slopes of the Bohemian Massif (southern Moravia, Czech Republic) and are known only from subsurface data that has been acquired for oil and gas exploration purposes.

- **Depositional environments** varied from a lower and middle shoreface to offshore, and the important role of storm events was revealed based on the facies analysis. The shoreline retreat due to erosion was significant with remobilisation of sediments in the form of tempestites. The role of bioturbation also highly varied.
- **Palynological study** implies the Late Albian age of studied deposits, and this connected them to the initial Cretaceous transgression (Albian–Lower Cenomanian) onto the Bohemian Massif. The base of the Klement Formation represents a composite, polyhistory surface and a subaerial unconformity. The thickness of Cretaceous deposits of the Klement Formation is generally increasing eastwardly.
- **Provenance** from the eastern margin of the Bohemian Massif is supposed for the Cretaceous deposits of the Klement Formation. Staurolite and garnet dominated the heavy

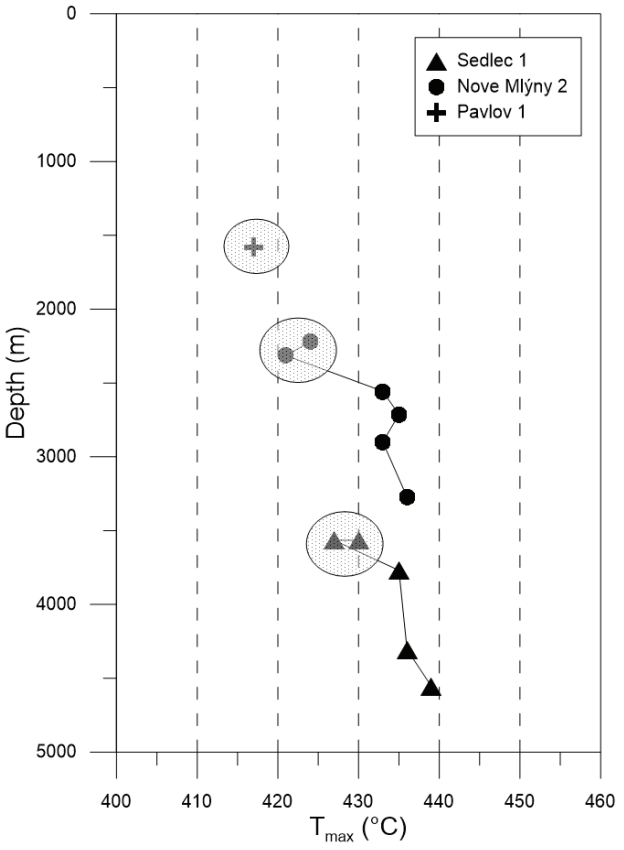

Fig. 17. Thermal maturity parameter (Tmax – maximum pyrolytic temperature) as a function of depth in the evaluated borehole profiles. Points in circles represent Cretaceous sediments of the Klement Formation, points without are from Mikulov Marls (Jurassic).

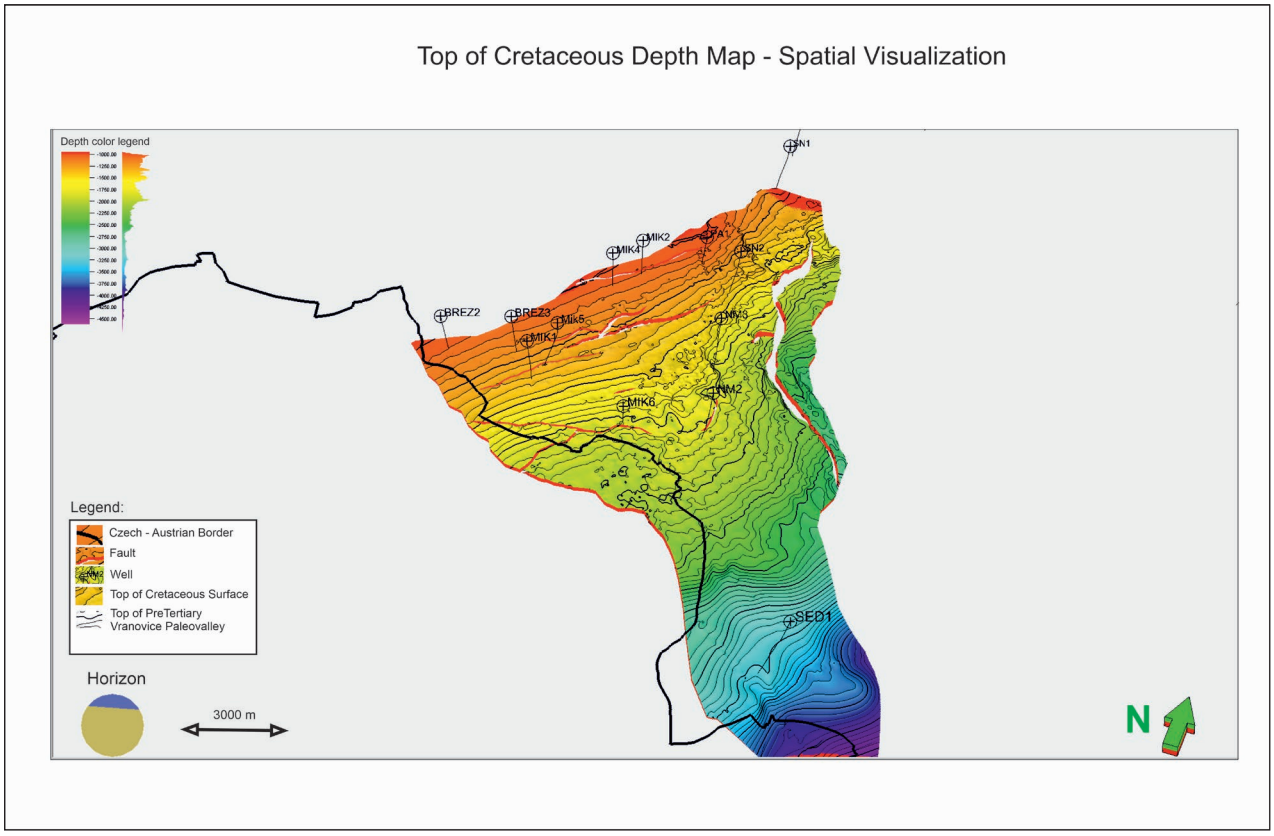

Fig. 18. Map on the top of Klement Formation.

mineral spectra, followed by kyanite. The superstable minerals (zircon, rutile and tourmaline) are significantly less common. The strong dominance of almandine–pyropes and pyrope–almandines in the garnet spectra was recognised. The rutile was mostly derived from pegmatites and metapelites (mica-schist, paragneiss, felsic granulite), whereas the role of metamafic rocks was less significant. The heavy minerals indicated relatively intense weathering patterns in the source area, formed by both crystalline schists and magmatic rocks (a mature continental crust). Detrital zircon age spectra reveals that the largest zircon population is of Paleozoic age being mostly Carboniferous and Devonian. The population of Carboniferous zircons is definitively dominated by Lower Carboniferous grains (mostly Tournasian), and the population of Devonian zircons is dominated by the upper Devonian (mostly Famenian) zircons; this confirms the important role of Variscan units in the source area. Younger zircons than 310.1 Ma are missing. A strong predominance of Neoproterozoic (mostly Ediacarian) zircons was observed within the Proterozoic zircon spectra, which confirms Cadomian units in provenance. The principal and proximal source can be traced to the geological unit of Moravo–Silesian Zone (Brunovistulicum), which composes the direct crystalline basement of these Mesozoic deposits. Slightly more distant sources can be traced to the Moravian and Moldanubian units or even more distant sources like the Teplá–Barrandian or Lugicum units.

- **The organic carbon content** (TOC) in the samples varied from 0.1 % to 0.4 %. Based on the TOC contents, all samples displayed a "poor" quality to generate hydrocarbons and the kerogen type III was typical for studied samples.

Acknowledgements: The authors wish to thank MND a.s. for providing the primary data and material support. The study was supported by the project NFP403201DNJ4 "Suistainable management of the subsurface waters in the area along the Czech–Slovak boundary" and by grant SP2025/086 from the Ministry of Education, Youth and Sports of the Czech Republic. We would like to thank Ondřej Bábek and Samuel Rybár for their helpful comments and suggestions, which improved the quality of the paper. We also thank associate editor Katarína Bónová for her remarks.

References

Adámek J. 1986: Geological data about the Mesozoic in the part South on the SE slope of the Bohemian Massif. *Zemní Plyn a Nafta, Hodonín* 31, 453–484 (in Czech).

Adámek J. 2005: The Jurassic floor of the Bohemian Massif in Moravia – geology and palaeogeography. *Bulletin of Geosciences* 80, 291–305.

Adámek J. & Stráník Z. 2021: Mezozoikum a paleogén platformy v předpolí Karpat. In: Stráník Z., Bubík M., Gilíková H. & Petrová T.P. (eds): Geologie Vnějších Západních Karpat a

jihovýchodního okraje Západoevropské platformy v České republice. *Česká geologická služba*, Praha, 52–68.

Adams J.S. & Weaver C.E. 1988: Thorium-to-Uranium ratios as indicators of sedimentary processes: example of concept of geochemical facies. *AAPG Bulletin* 2, 387–430.

Aubrecht R. & Méres Š. 2000: Exotic detrital pyrope–almandine garnets in the Jurassic sediments of the Pieniny Klippen Belt and Tatric Zone: where did they come from? *Mineralia Slovaca* 32, 17–28.

Aubrecht R., Méres Š., Sýkora M. & Mikuš T. 2009: Provenance of the detrital garnets and spinels from the Albian sediments of the Czorsztyn Unit (Pieniny Klippen Belt, Western Carpathians, Slovakia). *Geologica Carpathica* 60, 463–483. https://doi.org/10.2478/v10096-009-0034-z

Baniak G.M., Murray K., Gingras M.K., Beverly A., Burns B.A. & Pemberton S.G. 2013: An example of a highly bioturbated, storm-influenced shoreface deposit: Upper Jurassic Ula Formation, Norwegian North Sea. *Sedimentology* 61, 1261–1285. https://doi.org/10.1111/sed.12100

Brown A.R. 2004: Interpretation of Three-Dimensional Seismic Data, sixth edition. *AAPG Memoir* 42, 1–541.

Bucher K. & Frey M. 1994: Metamorphism of granitoids. In: Petrogenesis of Metamorphic Rocks: Complete Revision of Winkler's Textbook. *Springer*, Berlin, Heidelberg, 303–308.

Čech S. 2011: Paleogeography and stratigraphy of the Bohemian Cretaceous Basin (Czech Republic) - An overview. *Geologické výzkumy na Moravě a ve Slezsku* 1, 18–21

Čech S. & Valečka J. 1991: Významné transgrese a regrese v české křídové pánvi. *Manuscript, Ústřední ústav geologický*, 1–51.

Čech S., Klein V., Kříž J. & Valečka J. 1980: Revision of the Upper Cretaceous stratigraphy of the Bohemian Cretaceous Basin. *Věstník Ústředního ústavu geologického* 55, 277–296

Cháb J., Breiter K., Fatka O., Hladil J., Kalvoda J., Šimůnek Z., Štorch P., Vašíček Z., Zajíc J. & Zapletal. J. 2020: Stručná geologie základu Českého masivu a jeho karbonského a permského pokryvu. *Czech Geological Survey*, Praha, 1–283.

Ciprys V., Adamek J. & Benada S. 1995: Petroleum geology of the Carpathian Foredeep and overthrust zones in the Czech Republic. *Petroleum Geoscience* 1, 89–95. https://doi.org/10.1144/petgeo.1.1.89

Čopjaková R., Sulovský P. & Otava J. 2002: Comparison of the chemistry of detritic pyrope-almandine garnets of the Luleč Conglomerates with the chemistry of granulite garnets from the Czech Massif. *Geologické výzkumy na Moravě a ve Slezku v roce 2001,* Brno, 44–47 (in Czech).

Costa L.I. & Davey R.J. 1992: Dinoflagellate cysts of the Cretaceous System. In: Powell A.J. (Ed.): A Stratigraphic Index of Dinoflagellate Cysts. *Chapman & Hall*, London, 99–153.

Csiki-Sava Z., Buffetaut E., Ősi A., Pereda-Suberbiola X. & Brusatte S.L. 2015: Island life in the Cretaceous – faunal composition, biogeography, evolution, and extinction of land-living vertebrates on the Late Cretaceous European archipelago. *ZooKeys* 469, 1–161. https://doi.org/10.3897/zookeys.469.8439

Csontos L. & Vörös A. 2004: Mesozoic plate tectonic reconstruction of the Carpathian region. *Palaeogeography, Palaeoclimatology, Palaeoecology* 210, 1–56. https://doi.org/10.1016/j.palaeo.2004.02.033

Dinis P. & Castilho A. 2012: Integrating sieving and laser data to obtain bulk grain-size distributions. *Journal of Sedimentary Research* 82, 747–754. https://doi.org/10.2110/jsr.2012.62

Doveton J.H. 1991: Lithofacies and geochemical facies profiles from nuclear wireline logs: new subsurface templates for sedimentary modelling. In: Franseen E.K., Watney W.L., Kendall C.J. & Ross W. (eds.): Sedimentary modelling-computer simulations and methods for improved parameter definition. *Kansas Geological Society Bulletin* 233, 101–110.

Doveton J.H. & Merriam D.F. 2004: Borehole petrophysical chemostratigraphy of Pennsylvanian black shales in the Kansas subsurface. *Chemical Geology* 206, 249–258.

Eliáš M. 1981: Facies and paleogeography of the Jurassic of the Bohemian Massif. *Sborník Geologických Věd, Geology* 35, 75–144.

Espitalié J., Deroo G. & Marquis F. 1985: La pyrolyse Rock-Eval et ses applications. Premiere partie. *Revue du l'Institute Français du Petrole* 40, 563–579.

Fensome R.A. & Williams G.L. 2004: The Lentin and Williams index of fossil dinoflagellates. *American Association of Stratigraphic Palynologists, Contributions Series* 42, *AASP Publishers Press*, Salt Lake City, 1–909.

Finger F. & Haunschmid B. 1988: Die mikroskopische Untersuchung der akzessorischen Zirkone als Methode zur Klärung der Intrusionsfolge in Granitgebieten – eine Studie im nordöstlichen oberösterreichischen Moldanubikum. *Jahrbuch der Geologischen Bundesanstalt* 131, 255–266.

Finger F., Tichomirowa M., Pin C. & Hanžl P. 2000: Relics of an early-Panafrican metabasite–metarhyolite formation in the Brno Massif, Moravia, Czech Republic. *International Journal of Earth Sciences* 89, 328–335.

Force E.R. 1980: The provenance of rutile. *Journal of Sedimentary Research* 50, 485–488.

Frejková L. 1984: Petrografie sladkovodního cenomanu jv. okraje české křídové tabule. *Sborník GPO* 28, 87–112.

Frejková L. & Vajdík J. 1974: Příspěvek k paleogeografii a litologii cenomanských sedimentů v orlicko-žďárské faciální oblasti. *Sborník GPO* 6, 5–28.

Friedl G., Finger F., McNaughton N.J. & Fletcher I.R. 2000: Deducing the ancestry of terranes: SHRIMP evidence for South America-derived Gondwana fragments in central Europe. *Geology* 28, 1035–1038.

Friedl G., Finger F., Paquette J.L., von Quadt A., McNaughton N.J. & Fletcher I.R. 2004: Pre-Variscan geological events in the Austrian part of the Bohemian Massif deduced from U–Pb zircon ages. I*nternational Journal of Earth Sciences* 93, 802–823.

Geršlová E., Opletal V., Sýkorová I., Sedláková I. & Geršl M. 2015: A geochemical and petrographical characterization of organic matter in the Jurassic Mikulov Marls from the Czech Republic. *International Journal of Coal Geology* 141–142, 42–50. https://doi.org/10.1016/j.coal.2015.03.002

Geršlová E., Medvecká L., Jirman P., Nehyba S. & Opletal V. 2022: Source rock potential of the Miocene sedimentary rocks in the Carpathian Foredeep of the Czech Republic. *Geological Quarterly* 66, https://doi.org/10.7306/gq.1634

Gradstein F.M., Agterberg F.P., Ogg J.G., Hardenbol J., van Veen P., Thierry J. & Huang Z. 1995: A Triassic, Jurassic and Cretaceous time scale. In: Geochronology time scales and global stratigraphic correlation. *SEPM Special Publication* 54, 95–126.

Habryn R., Krzeminska E., Krzeminski L., Markowiak M. & Zielinski G. 2020: Detrital zircon age data from the conglomerates in the Upper Silesian and Małopolska blocks, and their implications for the pre-Variscan tectonic evolution (S Poland). *Geological Quarterly* 64, 321–341. https://doi.org/10.7306/gq.1539

Hanzlíková E. & Bosák P. 1977: Microfossils and microfacies of the Jurassic relict near Olomučany (Blansko district). *Věstník Ústředního ústavu* 52, 73–79.

Hanžl P., Janoušek V., Soejono I., Buriánek D., Svojtka M., Hrdličková K., Erban V. & Pin C. 2019: The rise of the Brunovistulicum: age, geological, petrological and geochemical character of the Neoproterozoic magmatic rocks of the Central Basic Belt of the Brno Massif. *International Journal of Earth Sciences* 108, 1165–1199.

Harms J.C., Southard J.B., Spearing D.R. & Walker R.G. 1975: Depositional environments as interpreted from primary sedi-

mentary structures and stratification sequences. *SEPM Short Course* 2, 1–161.

Hasseblo S.P. 1996: Stratigraphy, Cenozoic of the Atlantic margin, offshore New Jersey. In: Mountain G.S., Miller K.G., Blum P., Poag C.W. & Twichell D.C. (eds.): P*roceedings of the Ocean Drilling Program, Scientific Results* 150, 411–422.

Hrubcová P., Środa P., Grad M., Geissler W.H., Guterch A., Vozár J., & Hegedűs E. 2010: From the Variscan to the Alpine Orogeny: Crustal structure of the Bohemian Massif and the Western Carpathians in the light of the SUDETES 2003 seismic data. *Geophysical Journal International* 183, 611–633. https://doi.org/10.1111/j.1365-246X.2010.04766.x

Hubert J.F. 1962: A zircon-tourmaline-rutile maturity index and the interdependence of the composition of heavy mineral assemblages with the gross composition and texture of sandstones. *Journal of Sedimentary Petrology* 32, 440–450.

Jackson S.E., Pearson N.J., Griffin W.L. & Belousova E.A. 2004: The application of laser ablation-inductively coupled plasma-mass spectrometry to in situ U–Pb zircon geochronology. *Chemical Geology* 211, 47–69.

Jastrzębski M., Żelaźniewicz A., Murtezi M., Larionov A.N. & Sergeev S. 2015: The Moldanubian Thrust Zone – A terrane boundary in the Central European Variscides refined based on lithostratigraphy and U–Pb zircon geochronology. *Lithos* 220–223, 116–132. https://doi.org/10.1016/j.lithos.2015.01.023

Jastrzębski M., Żelaźniewicz A., Sláma J., Machowiak K., Śliwiński M., Jaźwa A. & Kocjan I. 2021: Provenance of Precambrian basement of the Brunovistulian Terrane: New data from its Silesian part (Czech Republic, Poland), central Europe, and implications for Gondwana break-up. *Precambrian Research* 355, 106108. https://doi.org/10.1016/j.precamres.2021.106108

Jirman P., Geršlová E., Bubík M., Sachsenhofer R.F., Bechtel A. & Więclaw D. 2019: Depositional environment and hydrocarbon potential of the Oligocene Menilite Formation in the Western Carpathians: a case study from the Loučka section (Czech Republic). *Marine and Petroleum Geology* 107, 334–350. https://doi.org/10.1016/j.marpetgeo.2019.05.034

Johnson H.D. & Baldwin C.T. 1986: Shallow siliciclastic seas. In: Reading H.G. (Ed.): Sedimentary environments and facies. *2nd edition, Blackwell Scientific Publ.,* Oxford, 229–282.

Klein V., Müller V. & Valečka J. 1979: Lithofazielle und paläogeographische Entwicklung des Böhmischen Kreidebeckens. Aspekte der Kreide Europas. *IUGS Series A* 6, 435–446.

Körmös S., Sachsenhofer R.F., Bechtel A., Rádovics B.G., Milota K. & Schubert F. 2021: Source rock potential, crude oil characteristics and oil-to-source rock correlation in a Central Paratethys sub-basin, the Hungarian Palaeogene Basin (Pannonian Basin). *Marine and Petroleum Geology* 127, 104955. https://doi.org/10.1016/j.marpetgeo.2021.104955

Kowal-Linka M., Jastrzębski M., Krzemińska E. & Czyput Z. 2022: The importance of parameter selection in studies of detrital zircon provenance: An example from Mesozoic deposits of the Bohemian Massif foreland (Poland). *Palaeogeography, Palaeoclimatology, Palaeoecology* 599, 111035. https://doi.org/10.1016/j.palaeo.2022.111035

Krejčí J. 1870: Studie v oboru křídového útvaru. I. Všeobecné a horopisné poměry, jakož i rozčlenění křídového útvaru v Čechách. *Archiv přírodovědecký, Výzkum Čech* 1, 35–161.

Krejčí O., Franců J., Müller P., Pereszlenyi M. & Straník Z. 1994: Geologic structure and hydrocarbon generation in the Carpathian flysch belt of south ern Moravia. Bulletin of the Czech *Geological Survey* 69, 13–26.

Krejčí O., Franců J., Poelchau H.S., Müller P. & Stráník Z. 1996: Tectonic evolution and oil and gas generation model in the contact area of the North European Platform with the West Carpathians. *EAGE Special Publication* 5, 177–186.

Krystek I. & Samuel O. 1978: Výskyt kriedy karpatského typu severně od Brna (Kuřim). *Geologické Práce, Správy* 71, 93–109.

Lafargue E., Marquis F. & Pillot D. 1998: Rock-Eval 6 applications in hydrocarbon exploration, production, and soil contamination studies. *Revue de l'Institut Français du Pétrole* 53, 421–437.

Leckie D.A. & Walker R.G. 1982: Storm- and tide dominated shorelines in Cretaceous Moosebar-Lower Gates interval: outcrop equivalents of Deep Basin gas trap in Western Canada. *AAPG Bulletin* 66, 138–157.

Leereveld H. 1995: Dinoflagellate cysts from the Lower Cretaceous Río Argos succession (SE Spain). *LPP contribution series* 2, 1–175.

Leszczyński S. & Nemec W. 2020: Sedimentation in a synclinal shallow-marine embayment: Coniacian of the North Sudetic Synclinorium, SW Poland. *The Depositional Record* 6, 144–161. https://doi.org/10.1002/dep2.92

Lihou J.C. & Mange-Rajetky M.A. 1996: Provenance of the Sardona Flysch, eastern Swiss Alps: example of high-resolution heavy mineral analysis applied to an ultrastable assemblage. *Sedimentary Geology* 105, 141–157.

Lindner M., Dörr W., Reither D. & Finger F. 2020: The Dobra Gneiss and the Drosendorf Unit in the southeastern Bohemian Massif, Austria: West Amazonian crust in the heart of Europe. *Geological Society, London, Special Publications* 503, SP503-2019-232.

Lindner M., Dörr W., Hauzenberger C.A., Reither D.& Finger F. 2021: In search of the oldest rock of Austria: The Hauergraben Gneiss, a 1.40 Ga old mafic quartz-monzonitic inlayer in the Dobra Gneiss (Drosendorf Unit, Bohemian Massif) as a new candidate. *Austrian Journal of Earth Sciences* 114, 29–45. https://doi.org/10.17738/ajes.2021.0002

Lister J.K. & Batten D.J. 1988: Stratigraphic and paleoenvironmental dististribution of early Cretaceous dinoflagellate cysts in the Hurlands farm borehole, West Sussex, England. *Palaeontographica, Abt. B* 210, 8–89.

Longhitano S.G. 2013: A facies-based depositional model for ancient and modern, tectonically–confined tidal straits. *Terra Nova* 25, 446–452.

MacEachern J.A. & Pemberton S.G. 1992: Ichnological aspects of Cretaceous shoreface successions and shoreface variability in the Western Interior Seaway of North America. In: Pemberton S.G. (Ed.): Applications of Ichnology to Petroleum Exploration. *SEPM Core Workshop* No. 17, Calgary, AB, 57–84.

Mader D. 1980: Weitergewachsene Zirkone im Bundsandstein der Westeifel. *Aufschluss* 31, 163–170.

Malkovský M., Benešová Z., Čadek J., Holub V., Chalopský J., Jetel J., Müller V., Mašín J. & Tásler R. 1974: Geologie české křídové pánve a jejího podloží. *Ústřední ústav geologický & Academia*, Praha, 1–262.

Mange M.A. & Morton A.C. 2007: Geochemistry of heavy minerals. In: Mange M.A. & Wright D.T. (eds.): Heavy Minerals in Use. *Developments in Sedimentology* 58, 345–391. https://doi.org/10.1016/S0070-4571(07)58013-1

Mayer J. & Sachsenhofer R.F. 2013: Shallow hydrocarbons in Lower Austria: A drilling hazard and a valuable exploration tool. *Austrian Journal of Earth Sciences* 106, 62–71.

Mazur S., Turniak K. & Bröcker M. 2004: Neoproterozoic and Cambro–Ordovician magmatism in the Variscan Kłodzko Metamorphic Complex (West Sudetes, Poland): new insights from U/Pb zircon dating. *International Journal of Earth Sciences (Geol. Rundsch.)* 93, 758–772. https://doi.org/10.1007/s00531-004-0417-4

Meinhold G., Anders B., Kostopoulos D. & Reischmann T. 2008: Rutile chemistra and thermometry as provenance indicator: An example from Chios Island, Grece. *Sedimentary Geology* 203, 98–111. https://doi.org/10.1016/j.sedgeo.2007.11.004

Méres Š., Aubrecht R., Gradiński M. & Sýkora M. 2012: High (ultra-high) pressure metamorphic terrane rocks as the source of the detrital garnets from the Middle Jurassic sands and sandstones of the Cracow Region (Cracow-Wieluń Upland, Poland). *Acta Geologica Polonica* 62, 231–245.

Mitchell A.J., Uličný D., Hampson G.J., Allison P.A., Gorman G.J., Piggott M.D., Wells M.R. & Pain C.C. 2010: Modelling tidal current-induced bed shear stress and palaeocirculation in an epicontinental seaway: the Bohemian Cretaceous Basin, Central Europe. *Sedimentology* 57, 359–388. https://doi.org/10.1111/j.1365-3091.2009.01082.x

Möller A., O'Brien P.J., Kennedy A. & Kröner A. 2003: Linking growth episodes of zircon and metamorphic textures to zircon chemistry: an example from the ultrahigh-temperature granulites of Rogaland (SW Norway). *Geological Society Special Publication* 220, 65–81.

Morton A.C. & Hallsworth C. 1994: Identifying provenance-specific features of detrital heavy mineral assemblages in sandstones. *Sedimentary Geology* 90, 241–256.

Myers K.J. & Wignall P.B. 1987: Understanding Jurassic organic-rich mudrocks – new concepts using gamma-ray spectrometry and palaeoecology: examples from the Kimmeridge Clay of Dorset and the Jet Rock of Yorkshire. In: Legget J.K. & Zuffa G.G. (eds.): Marine clastic sedimentology. *Graham and Trotman*, London, 172–189.

Nehyba S. & Opletal V. 2016: Depositional environment and provenance of the Gresten Formation (Middle Jurassic) on the south-eastern slopes of the Bohemian Massif (Czech Republic, subsurface data). *Austrian Journal of Earth Sciences* 109, https://doi.org/10.17738/ajes.2016.0020

Nehyba S. & Opletal V. 2017: Sedimentological study of the Nikolčice Formation – evidence of the Middle Jurassic transgression onto the Bohemian Massif (subsurface data). *Geological Quarterly* 61, 138–155. https://doi.org/10.7306/gq.1335

Nehyba S. & Šikula J. 2007: Depositional architecture, sequence stratigraphy and geodynamic development of the Carpathian Foredeep (Czech Republic). *Geologica Carpathica* 58, 53–69.

Opletal V., Geršlová E., Nehyba S., Sýkorová I. & Rez J. 2019: Geology and thermal maturity of Namurian deposits in the Němčičky Sub-basin as the south-eastern continuation of the Upper Silesian Coal Basin (Czech Republic). *International Journal of Coal Geology* 216, 303–323. https://doi.org/10.1016/j.coal.2019.103323

Otava J., Sulovský P. & Čopjaková O. 2000: Provenance changes of the Drahany Culm greywackes: statistical evaluation. *Geologické výzkumy na Moravě a ve Slezku v r. 1999*, Brno, 94–98 (in Czech).

Paton C., Woodhead J.D., Hellstrom J.C., Hergt J.M., Greig A. & Maas R. 2010: Improved laser ablation U–Pb zircon geochronology through robust downhole fractionation correction, Geochemistry Geophysics Geosystems 11, Q0AA06. https://doi.org/10.1029/2009GC002618

Pemberton S.G., Spila M., Pulham A.J., Saunders T., MacEachern J.A., Robbins D. & Sinclair I.K. 2001: Ichnology and Sedimentology of Shallow to Marginal Marine Systems: Ben Nevis and Avalon Reservoirs, Jeanne D'Arc Basin. *Geological Association of Canada*, St John's, NF, 1–343.

Peters K.E., Walters C.C. & Moldowan J.M. 2005: The biomarker Guide; I. Biomarkers and Isotopes in the Environment and Human History. II. Biomarkers and Isotopes in Petroleum Systems and Earth History. 2ed. *Cambridge University Press*, Cambridge.

Pícha F.J., Stránik Z. & Krejčí O. 2006: Geology and hydrocarbon resources of the Outer Western Carpathians and their foreland, Czech Republic. In: Golonka J. & Pícha F.J. (eds.): The Carpathians and their foreland: Geology and hydrocarbon resources: *AAPG Memoir* 84, 49–175.

Poldervaart A. 1950: Statistical studies of zircon as a criterion in granitization. *Nature* 165, 574–575.

Pupin J.P. 1980: Zircon and Granite Petrology. *Contributions to Mineralogy and Petrology* 73, 207–220.

Pupin J.P. 1985: Magmatic zoning of hercynian granitoids in France based on zircon typology. *Schweizerische Mineralogische und Petrographische Mitteilungen* 65, 29–56.

Řehánek J. 1978: Mikrofacie a mikrofauna písčito-glaukonitové série svrchní křídy z podloží karpatské předhlubně a vnějšího flyšového pásma na jižní Moravě. *Zemní Plyn a Nafta* 23, 327–346.

Řehánek J. 1984: The marine upper Albian of the Bohemian Massif in South Moravia (in Czech). *Geologické práce, Správy* 81, 87–101.

Řehánek J. 1995: Microfissils and palaeoenvironmental data on the Cenomanian/Turonian boundary in South Moravia (Czech Republic). In: Abstracts of the 2nd International Symposium on Cretaceous Stage Boundaries, Brussel, 98.

Rider M.H. 1991: The geological interpretation of well logs. Revised edition. *Whittles Publ.*, 1–175.

Rossi V., Perillo M., Steel R. & Olariu C. 2017: Quantifying mixed-process variability in shallow-marine depositional systems: What are sedimentary structures really telling us? *Journal of Sedimentary Research* 87, 1060–1074. https://doi.org/10.2110/jsr.2017.49

Ruffell A. & Worden R. 2000: Paleoclimatic analysis using spectral gamma-ray data from the Aptian (Cretaceous) of southern England and southern France. *Palaeogeography Palaeoclimatology Palaeoecology* 155, 265–283.

Rybár S. & Kotulová J. 2023: Petroleum play types and source rocks in the Pannonian Basin: Insight from the Slovak part of the Danube Basin. *Marine and Petroleum Geology* 149, 1–19. https://doi.org/10.1016/j.marpetgeo.2022.106092

Schmid S.M., Bernoulli D., Fügenshuh B., Mațenco L., Schefer S., Schuster R., Tischler M. & Ustaszewski K. 2008: The Alpine–Carpathian–Dinaridic orogenic system: Correlation and evolution of tectonic units. *Swiss Journal of Geosciences* 101, 139–183. https://doi.org/10.1007/s00015-008-1247-3

Skoček V. & Valečka J. 1983: Paleogeography of the Late Cretaceous Quadersandstein of the Central Europe. *Palaeogeography, Palaeoclimatology, Palaeoecology* 44, 71–92.

Skupien P., Smaržová A. & Měchová L. 2013: Palaeoenvironmental change in the Early Cretaceous Silesian Basin of the Western Carpathians (NE Czech Republic) inferred from palynological data. *Review of Palaeobotany and Palynology* 197, 143–151. https://doi.org/10.1016/j.revpalbo.2013.06.002

Sláma J., Košler J., Condon D.J., Crowley J.L., Gerdes A., Hanchar J.M., Horstwood M.S.A., Morris G.A., Nasdala L., Norberg N., Schaltegger U., Schoene N., Tubrett M.N. & Whitehouse M.J. 2008: Plešovice zircon – a new natural reference material for U–Pb and Hf isotopic microanalysis. *Chemical Geology* 249, 1–35.

Soejono I., Žáčková E., Janoušek V., Machek M. & Košler J. 2010: Vestige of an Early Cambrian incipient oceanic crust incorporated in the Variscan orogen: Letovice Complex, Bohemian Massif. *Journal of Geological Society (London)* 167, 1113–1130. https://doi.org/10.1144/0016-76492009-180

Soejono I., Schulmann K., Sláma J., Hrdličková K., Hanžl P., Konopásek J., Collett S. & Míková J. 2022: Pre-collisional crustal evolution of the European Variscan periphery: Constraints from detrital zircon U–Pb ages and Hf isotopic record in the Precambrian metasedimentary basement of the Brunovistulian Domain. *Precambrian Research* 372, 106606.

Stráník Z., Bubík M., Čech S. & Švábenická L. 1996: The Upper Cretaceous in south Moravia. *Věstník Českého geologického ústavu* 71, 1–30.

Stráník Z., Bubík M., Gilíková H. & Tomanová-Petrová P. 2021: Geologie Vnějších Západních Karpat a jihovýchodního okraje Západoevropské platform v České republice. *Česká geologická služba*, Praha, 1–319.

Svobodová M. 1992: Earliest Upper Cretaceous palynomorphs of basal (transgressive) strata in the Blansko Graben (Moravia, Czechoslovakia). In: Eder-Kovat J. (Ed.): Proceedings of the Pan-European Palaeobotanical Conference Vienna, 19–23 September 1991. *Museum of Natural History*, Vienna, 313–322.

Svobodová M. & Brenner G.J. 1999: Correlation of Mid-Cretaceous plant microfossils from the Raritan Formation of the Atlantic Coastal Plain with the Peruc-Korycany Formation of the Blansko Graben. *Acta Palaeobotanica, Supplement* 2, 199–209.

Taylor A.M. & Goldring R. 1993: Description and analysis of bioturbation and ichnofabric. *Journal of the Geological Society (London)* 150, 141–148.

Tocher B.A. & Jarvis I. 1987: Dinoflagellate cysts and stratigraphy of the Turonian (Upper Cretaceous) Chalk, near Beer, South-East Devon, England. In: Hart M.B (Ed.): Micropaleontology of carbonate environments. *Special Publication British Micropaleontological Society, Ellis Horwood*, Chichester, 138–175.

Tolosana-Delgado R., von Eynatten H. & Krippner A., Meinhold G. 2018: A multivariate discrimination scheme of detrital garnet chemistry for use in sediment provenance analysis. *Sedimentary Geology* 375, 14–26.

Triebold S., von Eynatten H., Luvizotto G.L. & Zack T. 2007: Deducing source rock lithology from detrital rutile geochemistry: An example from the Erzgebirge, Germany. *Chemical Geology* 244, 421–436.

Triebold S., von Eynatten H. & Zack T. 2012: A rec ipe for the use of rutile in sedimentary provenance analysis. *Sedimentary Geology* 282, 268–275.

Tyson R.V. 1995: Sedimentary organic Matter: Organic Facies and Palynofacies. *Chapman and Hall*, New York, 1–615.

Uličný D., Hladíková J., Attrep M., Čech S., Hradecká L. & Svobodová M. 1997: Sea-level changes and geochemical anomalies across the Cenomanian-Turonian boundary: Pecínov quarry, Bohemia. *Palaeogeography, Palaeoclimatology, Palaeoecology* 132, 265–285.

Uličný D., Laurin J. & Čech S. 2009a: Controls on clastic sequence geometries in a shallow-marine, transtensional basin: the Bohemian Cretaceous Basin, Czech Republic. *Sedimentology* 56, 1077–1114. https://doi.org/10.1111/j.1365-3091.2008.01021.x

Uličný D., Špičáková L., Grygar R., Svobodová M., Čech S. & Laurin J. 2009b: Palaeodrainage systems at the basal unconformity of the Bohemian Cretaceous Basin: roles of inherited fault systems and basement lithology during the onset of basin filling. *Bulletin of Geosciences* 84, 577–610. https://doi.org/10.3140/bull.geosci.1128

Valečka J. & Skoček V. 1990: Litoeventy v české křídové pánvi. *Věstník Ústředního ústavu geologického* 65, 13–28.

Voigt T. 1998: Entwicklung und Architektur einer fluviatilen Talfüllung – die Niederschöna Formation im Sächsischen Kreidebecken. *Abhandlungen des Staatlichen Museums für Mineralogie und Geologie in Dresden* 43/44, 121–139.

Voigt S., Wagreich M., Surlyk F., Walaszczyk I., Uličný D., Čech S., Voigt T., Wiese F., Wilmsen M., Niebuhr B., Reich M., Funk H., Michalík J., Jagt J.W.M., Felder P.J. & Schulp A.S. 2008: Cretaceous. In: McCann T. (Ed.): Geology of Central Europe. Volume 2: Mesozoic and Cenozoic. *Geological Society*, London, 923–998.

von Eynatten H. & Gaupp R. 1999: Provenance of Cretaceous synorogenic sandstones in the Eastern Alps: constraints from framework petrography, heavy mineral analysis and mineral chemistry. *Sedimentary Geology* 124, 81–111. https://doi.org/10.1016/S0037-0738(98)00122-5

Walker R.G. & James N.P. 1992: Facies Models: Response to Sea Level Changes. *Geological Association of Canada*, St. John's, 1–380.

Wessely G. 1988: Der Tiefenanschluss im Wiener Becken und der Molassenzone als Ausgangspunkt für die Alpenexploration in Österreich. *Erdöl Erdgas Kohle* 104, 440–446.

Wiedenbeck M., Alle P., Corfu F., Griffin W.L., Meier M., Oberli F., von Quadt A., Roddick J.C. & Spiegel W. 1995: Three natural zircon standards for U–Th–Pb, Lu–Hf, trace element and REE analyses. *Geostandards* 19, 1–23.

Williams G.L., Brinkhuis H., Pearce M.A, Fensome R.A. & Weegink J.W. 2004: Southern Ocean and Global Dinoflagellate Cyst Events Compared: Index Events for the late Cretaceous-Neogene. In: Exon N.F., Kennett J.P. & Malone M.J. (Eds): *Proceedings of the Ocean Drilling Program, Scientific Results* 189, 1–98.

Williams G.L., Fensome R.A. & MacRae R.A. 2017: The Lentin and Williams index of fossil dinoflagellates, 2017 edition. *AASP contributions series* 48, 1097.

Winter J. 1981: Exakte tephro-stratigraphische Korrelation mit morphologisch differenzierten Zironpopulationen (Grenzbereich Unter/Mitteldevon, Eifel-Ardennen). *Neues Jahrbuch für Geologie und Paläontologie, Abhandlungen* 162, 97–136.

Xiao Y., Rembe J., Čopjaková R., Aitchison J.C., Chen Y. & Zhou R. 2024: Sedimentary record of Variscan unroofing of the Bohemian Massif. *Gondwana Research* 128, 141–160. https://doi.org/10.1016/j.gr.2023.11.003

Zack T., von Eynatten H. & Kronz A. 2004a: Rutile geochemistry and its potential use in quantitative provenance studies. *Sedimentary Geology* 171, 37–58. https://doi.org/10.1016/j.sedgeo.2004.05.009

Zack T., Moraes R. & Kronz A. 2004b: Temperature dependence of Zr in rutile: empirical calibration of a rutile thermometer. *Contributions to Mineralogy and Petrology* 148, 471–488. https://doi.org/10.1007/s00410-004-0617-8

Zahajská P., Čepičková J., Trubač J., Pedentchouk N. & Kvaček J. 2024: The relationship of plant leaf $d^{13}C_{n\text{-alkanes}}$ and salinity on coastal ecosystems applied to paleobotany: Case study from the Cenomanian of the Bohemian Cretacesous Basin, Czechia. *Paleogeography, Paleoclimatology, Paleoecology* 638, 112052. https://doi.org/10.1016/j.palaeo.2024.112052

Żelaźniewicz A. & Fanning M. 2020: Neoarchean to Paleoproterozoic fragments in the Brunovistulia terrane, S Poland: a component of the Columbia Supercontinent? *Geological Quarterly* 64, 120–129.

Żelaźniewicz A., Buła Z., Fanning M., Seghedi A. & Żaba J. 2009: More evidence on Neoproterozoic terranes in Southern Poland and southeastern Romania. *Geological Quarterly* 53, 93–124.

Zimmerle W. 1979: Accessory Zircon from Rhyolite, Yellowstone National Park (Wyoming, U.S.A.). *Zeitschrift der deutschen Geologischen Gesellschaft* 130, 361–369.